OXFORD

Human Molecular Genetics, 2015, Vol. 24, No. 8 2330–2348

doi: 10.1093/hmg/ddu750
Advance Access Publication Date: 2 January 2015
Original Article

ORIGINAL ARTICLE

TBX1 protein interactions and *microRNA-96-5p* regulation controls cell proliferation during craniofacial and dental development: implications for 22q11.2 deletion syndrome

Shan Gao[1], Myriam Moreno[2,3], Steven Eliason[2,3], Huojun Cao[1], Xiao Li[2,3], Wenjie Yu[2,3], Felicitas B. Bidlack[4], Henry C. Margolis[5], Antonio Baldini[6] and Brad A. Amendt[2,3,*]

[1]Texas A&M University Health Science Center, Houston, TX, USA, [2]Department of Anatomy and Cell Biology, [3]Craniofacial Anomalies Research Center, The University of Iowa, Iowa City, IA, USA, [4]Department of Mineralized Tissue Biology, [5]Center for Biomineralization, Department of Applied Oral Sciences, The Forsyth Institute, Cambridge, MA, USA and [6]Department of Molecular Medicine and Medical Biotechnology, University Federico II and the Institute of Genetics and Biophysics CNR, Naples, Italy

*To whom correspondence should be addressed. Tel: +1 3193353694; Fax: +1 3193357770; Email: brad-amendt@uiowa.edu

Abstract

T-box transcription factor *TBX1* is the major candidate gene for 22q11.2 deletion syndrome (22q11.2DS, DiGeorge syndrome/Velo-cardio-facial syndrome), whose phenotypes include craniofacial malformations such as dental defects and cleft palate. In this study, *Tbx1* was conditionally deleted or over-expressed in the oral and dental epithelium to establish its role in odontogenesis and craniofacial developmental. Tbx1 lineage tracing experiments demonstrated a specific region of Tbx1-positive cells in the labial cervical loop (LaCL, stem cell niche). We found that *Tbx1* conditional knockout ($Tbx1^{cKO}$) mice featured microdontia, which coincides with decreased stem cell proliferation in the LaCL of $Tbx1^{cKO}$ mice. In contrast, *Tbx1* over-expression increased dental epithelial progenitor cells in the LaCL. Furthermore, *microRNA-96* (*miR-96*) repressed *Tbx1* expression and Tbx1 repressed *miR-96* expression, suggesting that *miR-96* and Tbx1 work in a regulatory loop to maintain the correct levels of *Tbx1*. Cleft palate was observed in both conditional knockout and over-expression mice, consistent with the craniofacial/tooth defects associated with *TBX1* deletion and the gene duplication that leads to 22q11.2DS. The biochemical analyses of *TBX1* human mutations demonstrate functional differences in their transcriptional regulation of *miR-96* and co-regulation of PITX2 activity. TBX1 interacts with PITX2 to negatively regulate PITX2 transcriptional activity and the TBX1 N-terminus is required for its repressive activity. Overall, our results indicate that Tbx1 regulates the proliferation of dental progenitor cells and craniofacial development through *miR-96-5p* and PITX2. Together, these data suggest a new molecular mechanism controlling pathogenesis of dental anomalies in human 22q11.2DS.

Received: October 23, 2014. **Revised and Accepted:** December 30, 2014

Introduction

22q11.2 deletion syndrome (22q11.2DS) is the unifying term for patients with a common microdeletion on one of the proximal long arms of chromosome 22. This deletion encompasses the genes responsible for DiGeorge syndrome (DGS, MIM#188400), velo-cardio-facial syndrome (VCFS, MIM# 192430) and conotruncal anomaly face syndrome. Characteristic features include congenital heart defects, hypoplasia or aplasia of the thymus and parathyroid and craniofacial dysmorphisms including tooth defects (1–3). Three research groups identified *Tbx1* as the candidate gene for 22q11.2DS based on the analyses of segmental deletions and single gene knockout mice (4–6). Although the extensive evidence gathered from these mouse studies and information on human *TBX1* mutations strongly support *TBX1* as the candidate gene involved in 22q11.2DS, the molecular mechanisms underlying the loss or gain of *TBX1* function in the pathogenesis of 22q11.2DS is not fully understood.

Tbx1 is a member of the T-box gene family, a group of evolutionarily conserved transcription factors that share a 180–200 amino acid DNA binding domain called the T-box (7). The expression pattern of *Tbx1* is consistent with the critical role *Tbx1* plays during pharyngeal apparatus formation, heart development and tooth morphogenesis (8–10). Moreover, mouse studies have associated a progressive reduction in dosage of the *Tbx1* mRNA with a non-linear increase in severity of the phenotype (11), and an increase in *Tbx1* mRNA dosage with malformations similar to those observed in 22q11.2DS patients (12,13). Recent studies suggest that Tbx1 plays a role in the regulation of several myogenic genes associated with core mesoderm cell survival and fate required for the formation of the branchiomeric muscles (14). $Tbx1^{Cre}$ fate mapping experiments from E10.5 to E14.5 reveal Tbx1 positive cells in tooth buds and surface ectoderm (15). These findings highlight the need for precise regulation of *Tbx1* expression during embryogenesis.

Because DGS patients have dental anomalies we used *Tbx1* conditional knockout mice, over-expression mice and $Tbx1^{Cre}$ mice to determine the molecular basis for dental defects in DGS. The mouse dentition is unique in that the incisor continually grows through the life of the mouse while the molars do not. Each incisor has two cervical loops (CLs), one on the labial side (LaCL) and the other on the lingual side (LiCL). The epithelial stem cells on the incisor reside in the LaCL, which consists of the stellate reticulum (SR), the inner enamel epithelium (IEE) and the outer enamel epithelium (OEE). The self-renewing stem cells localize to the SR and these stem cells will give rise to transit-amplifying (T-A) cells that differentiate into mature enamel-secreting ameloblasts. This process is necessary for matrix deposition and subsequent enamel mineralization (16,17). Many 22q11.2DS patients suffer from enamel hypoplasia, hypomineralization, hypodontia, delayed tooth eruption and excessive dental caries (3). At E11.5, *Tbx1* is expressed in the oral epithelium and during early incisor development, it is expressed in the IEE, OEE, CLs and enamel knot (Ek), and at later stages, it is localized to the IEE in molars and incisors (10).

Recent studies have examined the role of microRNAs (miRs) in tooth development. Discrete sets of miRs are expressed in molars compared with incisors, epithelial compared with mesenchymal compartments of the incisors and differentiated ameloblasts compared with cells of the LaCL (18,19). One study compared miRs expressed in the LaCL, the LiCL and enamel-producing ameloblasts (20). These studies confirm that discrete cohorts of miRs regulate the incisor stem cell niche versus ameloblast maturation.

In this report, we show that Tbx1 and *miR-96* interact in a negative regulatory loop to maintain the correct dose of Tbx1 in the dental epithelium and that *Tbx1* regulates the proliferation of epithelial progenitor stem cells in the LaCL. We demonstrate new Tbx1 protein interactions and a molecular basis for human *TBX1* mutations in the regulation of tooth and craniofacial development. This study reveals *Tbx1* to play a central role in the pathway that regulates tooth and craniofacial development in adult mice, with changes in *Tbx1* dosage in the dental epithelium affecting tooth size, molar cusping, ameloblast differentiation and enamel production.

Results

miR-96-5p regulates *Tbx1* expression in the dental epithelium

miRs play a critical role in the regulation of tooth stem cell proliferation and differentiation (18,20–23). A schematic representation of the mouse lower incisor (LI) and cells that populate the growing incisor during tooth development, including the LaCL (the stem cell niche), is shown (Fig. 1A). The mouse dental epithelium (light blue, which includes the LaCL and ameloblasts, Am) was extracted and the LaCL cells were isolated from the ameloblast cells and used to analyze miR expression. Analyses of miR expression during LI development at P0 showed low *miR-96-5p* expression in the LaCL, however, *miR-96-5p* expression increased >2-fold in the differentiating pre-ameloblast and ameloblast cells (Fig. 1B). The *Tbx1* 3′UTR contains a highly conserved *miR-96* binding element, which was cloned into a luciferase reporter to assess *miR-96* function (Fig. 1C). *miR-96* repressed luciferase expression from the WT *Tbx1* 3′UTR, but not from a mutated *Tbx1* 3′UTR, in LS-8 oral epithelial cells (Fig. 1D). Over-expression of *miR-96* in LS-8 cells repressed endogenous *Tbx1* expression, as shown by real-time PCR (Fig. 1E). Western blots of *miR-96* transfected LS-8 cells demonstrated decreased Tbx1 protein, while cells transfected with empty vector or a scrambled miR did not show a change in *Tbx1* expression (Fig. 1F). Together these data demonstrate that *miR-96* represses Tbx1 and correlates with high levels of *Tbx1* expression in the LaCL (low levels of *miR-96*). Interestingly, a miR screen in *Tbx1* over-expression mice ($COET^{K14Cre}$) mandibles revealed a decrease in *miR-96* expression compared with wild-type (WT). Real-time PCR confirmed decreased *miR-96* expression in $COET^{K14Cre}$ mice mandible (Fig. 1G). Thus, we have tentatively identified a *Tbx1-miR-96* feedback loop, where *miR-96* represses *Tbx1* and Tbx1 represses *miR-96* expression.

The Tbx1 N-terminus is required for repression of PITX2 transcriptional activity

We have previously shown that Tbx1 interacts with the PITX2 C-terminus to repress PITX2 transcriptional activity (24). However, the Tbx1 domain for protein interactions was not known. We generated a series of Tbx1 truncated proteins to test for PITX2 interactions and transcriptional activity (Fig. 2A). GST-Tbx1 pull-down experiments demonstrate that PITX2 binds to the N-terminus of Tbx1 (Fig. 2B). PITX2 protein (500 ng) was incubated with GST-Tbx1 FL (full-length) and truncated proteins to determine the protein interaction domain of Tbx1. PITX2 bound to Tbx1 FL, Tbx1 ΔC and Tbx1 ΔTC, but not to Tbx1 T-box or Tbx1 ΔNT. PITX2 did not bind to Tbx1 ΔN (data not shown). The

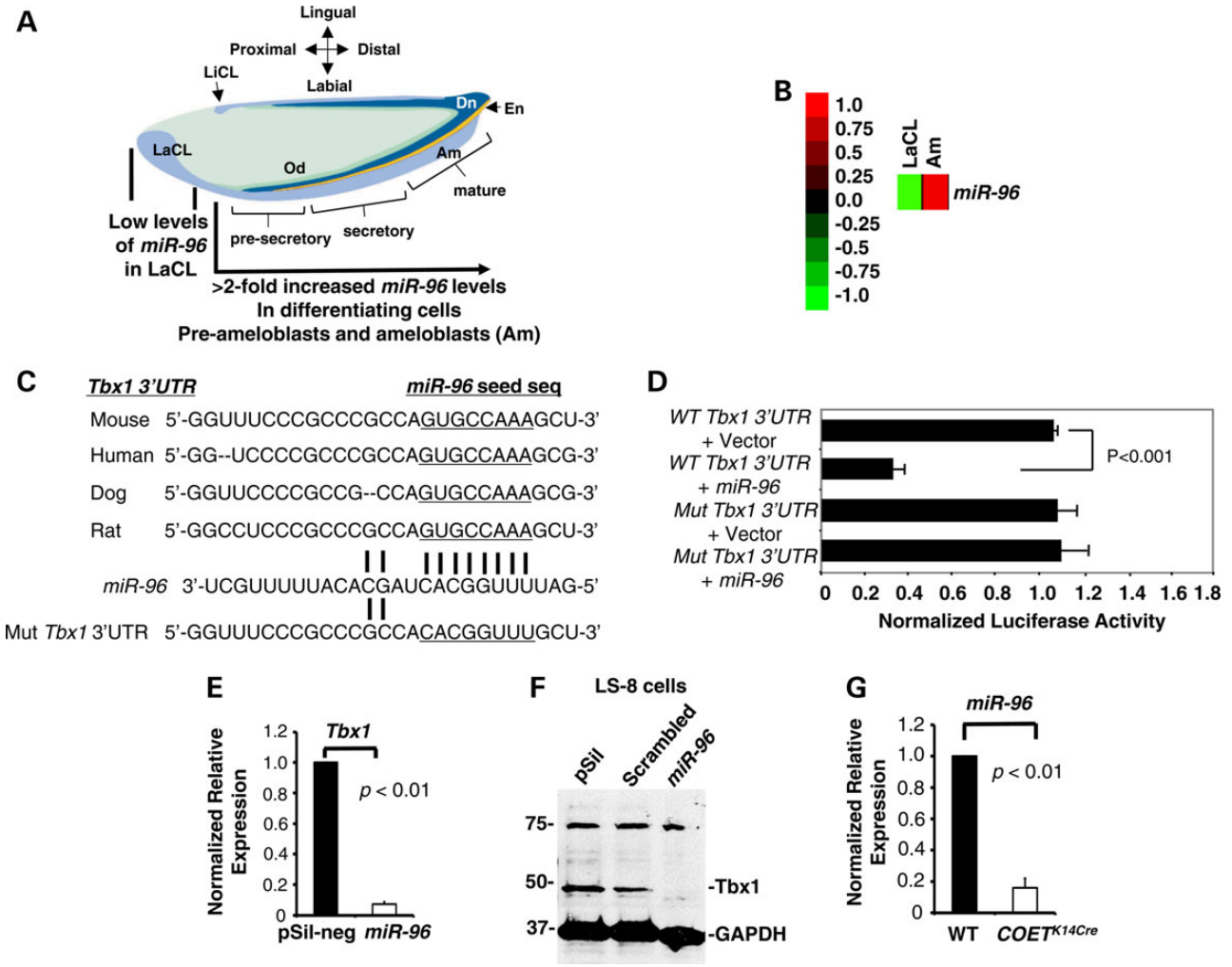

Figure 1. *miR-96* targets Tbx1 and Tbx1 represses *miR-96* expression. (**A**) Schematic depiction of the mouse LI. *miR-96* is expressed at low levels in the LI LaCL, but increased in the differentiating ameloblast cells. Dn, dentin; En, enamel; Am, ameloblasts; Od, odontoblasts; LaCL, labial cervical loop; LiCL, lingual cervical loop. (**B**) Heat map of *miR-96* differentially expressed between the LaCL (stem cell niche) and Am (differentiating cells) region. Five biological samples were assayed for each region, and one sample is shown. (**C**) The *Tbx1* 3′UTR *miR-96* binding site is highly conserved among species. The sequence of this region that is mutated in the Mut *Tbx1* 3′UTR (*miR-96* seed seq.; underlined) results in an inability to bind *miR-96*. (**D**) Normalized luciferase activity of the 3′-UTR *Tbx1*-luciferase reporter (WT *Tbx1* 3′*UTR*) in the presence of empty plasmid (Vector) or CMV-*miR-96* (*miR-96*) shows that luciferase activity is lost when *miR-96* is expressed; this is not the case when the *miR-96* seed sequence is mutated (Mut *Tbx1* 3′UTR). Error bars indicate ± SEM, five independent experiments ($n = 5$); $P < 0.001$. (**E**) Expression of *miR-96* in LS-8 oral epithelial cells repressed endogenous *Tbx1* expression. Real-time PCR experiments measured *Tbx1* transcripts with and without *miR-96* expression and normalized to control gene ($N = 3$). (**F**) Western blot analysis shows that Tbx1 levels decrease when *miR-96* is over-expressed in LS-8 oral epithelial-like cells. GAPDH served as a loading control. (**G**) Tooth germ RNA isolated from WT and $Tbx1^{K14COET}$ mice mandibles demonstrated significantly decreased *miR-96* expression. Real-time PCR was performed on three biological samples and each experiment was performed in triplicate ($N = 3$).

PITX2 binding domain was localized to the N-terminus of Tbx1 (Fig. 2A and B).

PITX2 activates the mouse *Pitx2c* promoter in LS-8 oral epithelial cells and auto-regulates its expression (Fig. 2C) (24). Tbx1 FL, Tbx1 ΔC and Tbx1 ΔN proteins do not activate the *Pitx2c* promoter; however, both Tbx1 FL and Tbx1 ΔC repress PITX2 activation of the Pitx2c promoter (Fig. 2C). Deletion of Tbx1 N-terminus (Tbx1 ΔN) does not activate the Pitx2c promoter and does not repress PITX2 transcriptional activity, as would be expected as the Tbx1 N-terminus interacts with PITX2 (Fig. 2C). The Tbx1 truncated proteins were expressed in LS-8 cells (Fig. 2D). Thus, the Tbx1 N-terminus is a site for protein interactions and we show that the Tbx1 N-terminus is required to repress PITX2 transcriptional activity. Furthermore, cells transfected with Tbx1 FL showed decreased endogenous Pitx2 expression (Fig. 2E).

Human *TBX1* mutations have variable activity

TBX1 mutants associated with 22q.11.2DS bind DNA and we have shown that Tbx1 interactions with PITX2 do not alter PITX2 DNA binding (24–27). However, one report shows that TBX1 mutant proteins F148Y, H194Q and G310S activate an artificial promoter, with TBX1 H194Q having increased transcriptional activity compared with WT TBX1 (25). Two other reports using artificial reporters (CAT and luciferase reporters with T-Box sites or Brachyury consensus binding site sequences) show reduced or no activation of the reporters with the mutant proteins compared with WT TBX1 (26,27). We also tested TBX1 and mutants with an artificial luciferase reporter (contains T-Box elements from the FGF promoter) and found little activation by WT or mutant proteins (data not shown). However, we asked if the TBX1 mutants altered

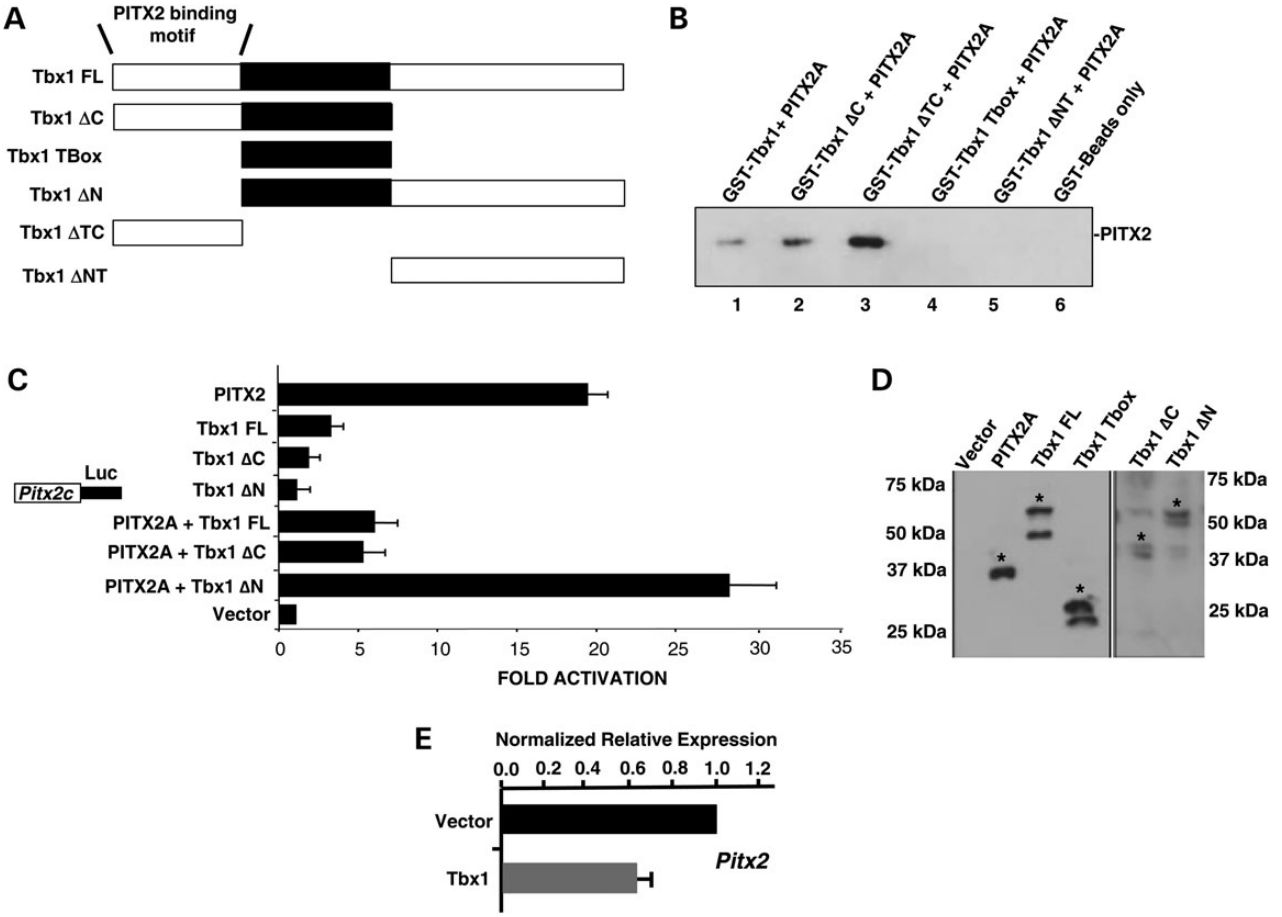

Figure 2. The Tbx1 N-terminus is required for PITX2 interaction and repression of PITX2 transcriptional activity. (**A**) A schematic of the Tbx1 truncated proteins used in the GST pull-down and transfection assays. The black shaded region is the T-box DNA binding domain. (**B**) GST pull-down using GST-Tbx1 truncated proteins to bind purified PITX2 protein. The PITX2 bound protein was resolved on 10% PAGE gel transferred to PVDF filters, immunoblotted and detected using PITX2ABCDE antibody (Capra Science, Sweden) and ECL reagents. PITX2 bound to Tbx1 full-length (FL), Tbx1ΔC (C-terminus deleted) and Tbx1ΔTC (T-box and C-terminus deleted). PITX2 did not bind to the Tbx1 T-box (Tbx1T-box) or Tbx1 C-terminus (Tbx1ΔNT), also PITX2 did not bind to Tbx1ΔN (data not shown). (**C**) Tbx1 truncations were tested in transfection assays to determine their activity and ability to repress PITX2 transcriptional activation of the Pitx2c promoter. As expected Tbx1 activated the Pitx2c promoter at low levels and the Tbx1ΔC and Tbx1ΔN proteins did not activate the promoter. However, deletion of the Tbx1 N-terminus (Tbx1ΔN) did relieve the repressive effect of Tbx1 on PITX2 transcriptional activation of the Pitx2c promoter. Luciferase activity is shown as mean-fold activation compared with activity in the context of the empty expression plasmid (Vector). All luciferase activities were normalized to β-galactose expression; five independent experiments were performed in LS-8 cells ($N = 5$). (**D**) Western blot of transfected cells to show expression in transfected LS-8 cells. Whole-cell lysates (30 μg) were resolved on 10% polyacrylamide gels, and PITX2 and Tbx1 truncated proteins were detected using an antibody against the Myc tag. All Tbx1 truncated proteins were expressed and denoted by an asterisk. (**E**) Real-time PCR experiments from cells transfected with Tbx1 or empty vector demonstrate decreased levels of endogenous *Pitx2* transcripts by Tbx1 over-expression ($N = 3$).

PITX2 transcriptional activity. A schematic representation of the *TBX1* gene and mutations is shown (Fig. 3A). TBX1 has three isoforms, A, B and C with C being the most conserved between mice and humans and the most highly expressed in humans (28,29). To determine if these mutants repressed PITX2 transcriptional activity PITX2 was transfected at 1 μg and TBX1 plasmids at 0.25, 0.5 and 1 μg s, respectively. Interestingly, human TBX1 variant C (VC) showed a slight activation of the *Pitx2c* promoter in LS-8 cells (Fig. 3B). However, both TBX1 VC and TBX1 G310S (G-S) mutant proteins repressed PITX2 transcriptional activation of the *Pitx2c* promoter (Fig. 3B). TBX1 G-S and TBX1 H194Q (H-Q) mutant proteins did not activate the *Pitx2c* promoter. Interestingly, the TBX1 H-Q protein did not repress PITX2 activation (Fig. 3B). In previous reports, the stability of the TBX1 mutant proteins was not analyzed, and we found that both TBX1 G-S and H-Q were expressed and stable in the LS-8 cells. Because PITX2 interacts with the N-terminus of Tbx1 and Tbx1 interacts with the C-terminus of PITX2 the loss of TBX1 repression of PITX2 with the H-Q mutation suggests other protein functions. Further experiments are required to determine the exact mechanisms. These data could explain phenotypic variations among 22q.11.2DS patients.

Tbx1 binds to the *miR-96* promoter and represses *miR-96* expression

To confirm Tbx1 regulation of *miR-96*, a chromatin immunoprecipitation (ChIP) assay was performed to demonstrate endogenous Tbx1 binding to the *miR-96* chromatin. A Tbx1 binding site was identified 3251 base pairs upstream of the *miR-96* transcription start site (Fig. 4A). This Tbx1 binding site is similar to a recent report that identified Tbx1 binding sites by SELEX (27). As a control, primers were designed to a site upstream of the Tbx1 binding element in the *miR-96* promoter and this DNA was not immunoprecipitated (IP'ed) by IgG serum or Tbx1 antibody (Fig. 4A, lanes 2 and 3, respectively). However, the Tbx1 antibody

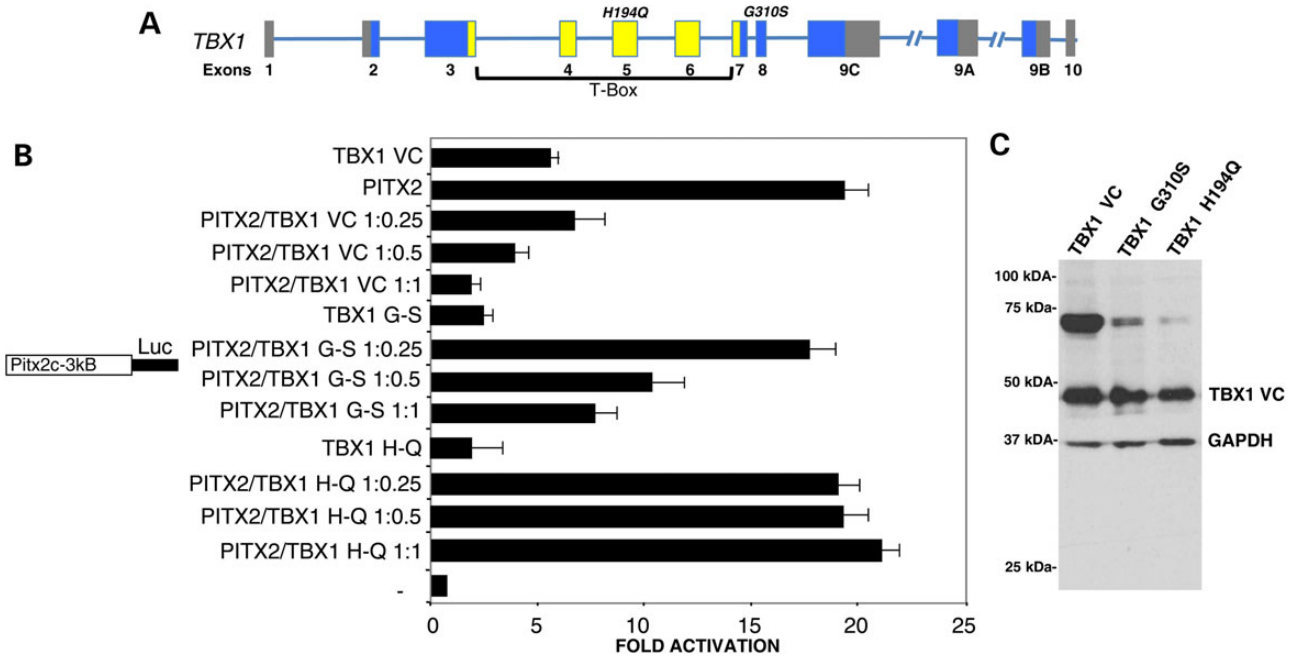

Figure 3. TBX1 human mutants differentially regulate PITX2 transcriptional activity. (**A**) Schematic representation of human TBX1 isoforms and mutations. TBX1C, TBX1A and TBX1B are made by alternative splicing of the last exons and the T-box is shown. (**B**) TBX1 VC (variant C), TBX1 G310S (G-S) and TBX1 H194Q (H-Q) were transfected or cotransfected with PITX2 and the Pitx2c promoter. Each transfection used 0.1 μg reporter, 0.1 μg PITX2 and 0.25, 0.05, 0.1 μg of the TBX1 construct. To control for transfection efficiency, all transfections included the SV-40 β-galactosidase reporter (0.05 μg). Cells were incubated for 24 h and then assayed for luciferase and β-galactosidase activities. The activities are shown as mean-fold activation compared with the luciferase plasmid with empty vector and normalized to β-galactosidase activity ±SE from three independent experiments. TBX1 VC slightly activated the Pitx2c promoter (6-fold) and showed a dose-responsive repression of PITX2 transcriptional activity. TBX1 G-S did not activate the Pitx2c promoter and also showed a dose-responsive repression of PITX2 activity albeit at lower levels compared with WT TBX1 VC. However, TBX1 H-Q did not activate the Pitx2c promoter or repress PITX2 transcriptional activation of the Pitx2c promoter. (**C**) Western blots of transfected LS-8 cells to demonstrate expression levels of TBX1 mutant proteins. Whole-cell lysates (30 μg) were resolved on 10% polyacrylamide gels, and TBX1 mutant proteins were detected using an antibody against the Myc tag. GAPDH served as a loading control. TBX1 VC, TBX1 G-S and TBX1 H-Q transfected proteins were expressed in the cells.

did IP the DNA containing the Tbx1 binding element (Fig. 4A, lane 7).

The *miR-96* promoter was cloned (~5 kb) into the luciferase vector to test for Tbx1 functional regulation. Murine Tbx1, human TBX1 VC and TBX1 G-S all repressed the *miR-96* promoter (4-fold or greater, $P < 0.05$), while TBX1 H-Q had no effect (Fig. 4B). Furthermore, because TBX1 H-Q binds DNA (27), the inability of this mutant to repress the miR-96 promoter could suggest defective protein interactions, other than PITX2. Thus, Tbx1 directly represses *miR-96* expression and this is the first demonstration of Tbx1 repression of a miR.

Because Tbx1 repressed PITX2 transcriptional activation, we reasoned that *miR-96* indirectly modulated PITX2 transcriptional activity through the regulation of Tbx1. LS-8 cells co-transfected with *miR-96* and the *Pitx2c* promoter revealed no activation; however, co-expression of PITX2 and *miR-96* increased PITX2 activation of the *Pitx2c* promoter, compared with PITX2 alone (Fig. 4C). Thus, *miR-96* repression of Tbx1 indirectly activates PITX2 transcriptional activity.

Specific *Tbx1* expression in the incisor CL controls incisor development

The rodent incisor is a unique model for the differentiation of enamel organ cells from stem cells to enamel-secreting ameloblasts (Fig. 5A). Stem cells located in the LaCL give rise to the pre-secretory, secretory and maturation-stage epithelial or ameloblast cells.

Tbx1 was conditionally knocked out using the $K14^{Cre}$ mouse crossed to the $Tbx1^{f/f}$ mouse to generate the $Tbx1^{K14cKO}$ *mice*. The *K14* promoter is active in surface ectoderm and basal cells from embryonic day E9.5 in developing hair follicles and tooth epithelia (30–32). At P0, the LI LaCL was smaller and disorganized in $Tbx1^{K14cKO}$ mice compared with WT, and the inner enamel epithelial (IEE) cells appeared undifferentiated and not well polarized (Fig. 5B and C). Furthermore, the OEE and stratum intermedium (SI) layer was thin, unorganized and lacked structure (Fig. 5C).

Tbx1 transcripts were specific to the dental epithelium in both the incisors and molars and were detected from E10.5 to E18.5 (10,33,34). Tbx1 protein expression in teeth was confirmed by immunofluorescence of the LI at E16.5 and Tbx1 was expressed in the myogenic core of the tongue (t), dental follicle, dental lamina, oral epithelium and in both the LaCL and LiCL (Fig. 5D–I). Tbx1 expression was seen in the IEE, OEE and SR of the LaCL (Fig. 5H and I). However, Tbx1 expression decreased in differentiating ameloblasts and was not seen in the odontoblasts.

The $Tbx1^{Cre}$ mouse was crossed with the $ROSA26^{LacZ}$ reporter mouse to better understand Tbx1 cell fate during incisor development. Fate mapping of Tbx1-expressing cells revealed Tbx1-expressing cells specifically in the LaCL of the LI. High magnification imaging of the LaCL indicated that Tbx1-expressing cells populated the distal region of the SR, and in the OEE and IEE (Fig. 5J). The stem cells located in the SR compartment intercalate into the OEE and move around the CL to the IEE, where they divide and migrate to the distal part of the growing incisor (35) (see arrows, Fig. 5J). Interestingly, cells in the proximal SR were Tbx1

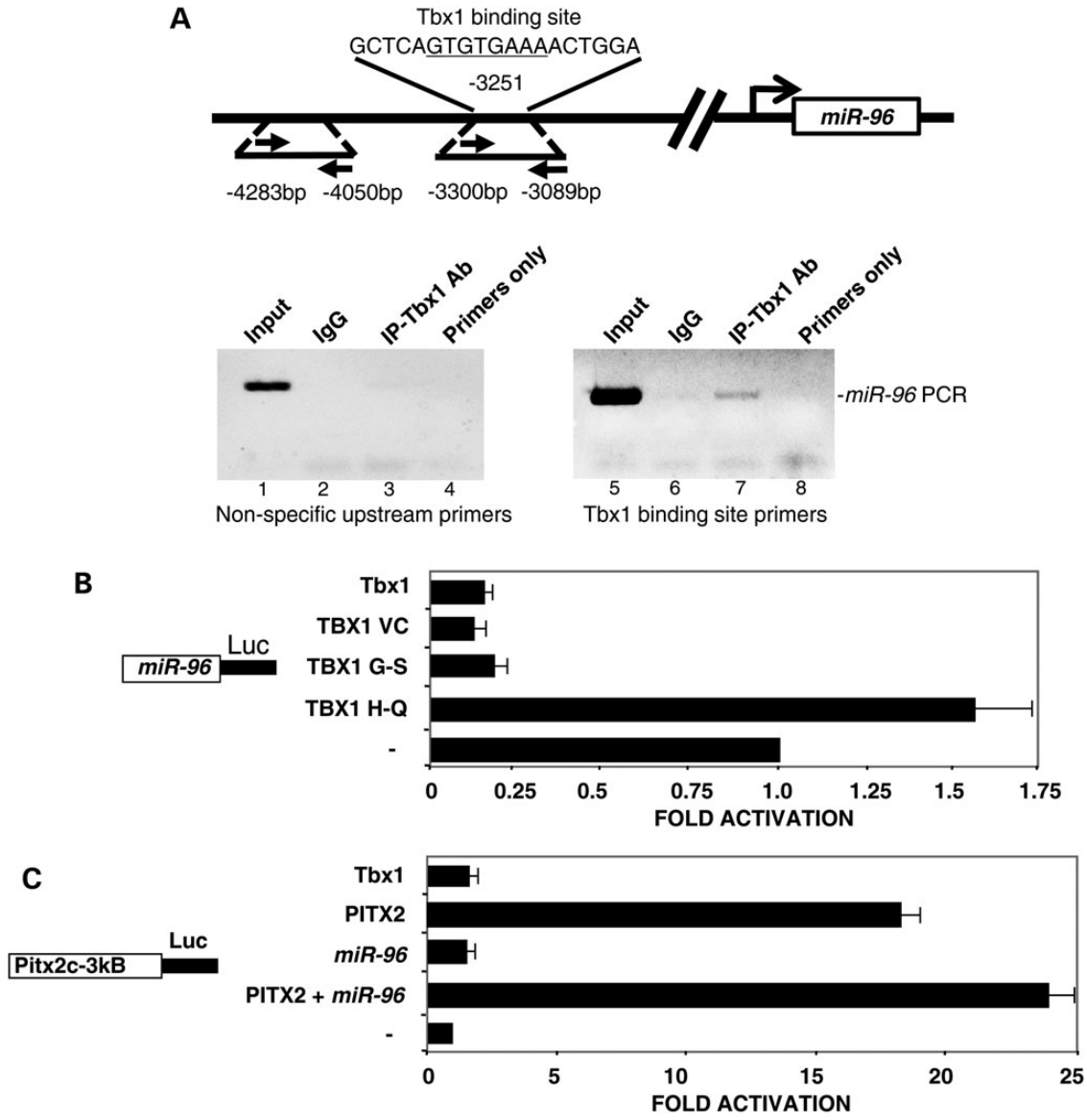

Figure 4. Endogenous Tbx1 binds to the *miR-96* chromatin. (**A**) Top panel is a schematic representation of the miR-96 5′-flanking region upstream of *pri-miR-96*. The Tbx1 binding site is shown and the primer regions used to amplify the chromatin as well as the control primers upstream of the Tbx1 binding site. Bottom panels, ChIP of endogenous Tbx1 binding to the T-box element upstream of the *pri-miR-96* transcript in LS-8 cells, lane 7. IgG did not IP the Tbx1 binding site chromatin, lane 6. IgG and Tbx1 Ab did not IP the control region (non-specific primers) upstream of the Tbx1 binding sequence, lanes 2 and 3, respectively. Rabbit antisera was used as a control IP and Tbx1 antibody (Invitrogen) was used to IP Tbx1 binding to the chromatin. The input chromatin is shown as a positive control for the ChIP. (**B**) Expression plasmids containing the murine Tbx1, human TBX1 variant C, TBX1 G310S and TBX1 H194Q cDNAs were co-transfected into LS-8 cells with the *miR-96* 5 kb luciferase reporter plasmid. Luciferase activity is shown as mean-fold activation compared with that in the presence of empty mock expression plasmid. All luciferase activities were normalized to β-galactose expression, three independent experiments ($N = 3$). (**C**) Tbx1, PITX2 and *miR-96* were co-transfected in LS-8 cells with the *Pitx2c* luciferase promoter and luciferase activity measured as in Figure 2. All luciferase activities were normalized to β-galactose expression, three independent experiments ($N = 3$).

negative (Fig. 5J). Tbx1 daughter cells were observed in the differentiating ameloblasts or secretory cells and in the SI (Fig. 5K). Overall, these results suggest that Tbx1 marks a specific subset of dental epithelial stem cells in the LaCL, different and independent from Sox2 (36).

Abnormal tooth development and amelogenin expression in $Tbx1^{K14cKO}$ mutant embryos and neonate mice

The differentiation of dental epithelial cells into ameloblasts occurs through several morphological stages, over this period the cells become elongated and polarized, features that are required for the deposition of enamel (37).

In this report we used *Tbx1* conditionally deleted mice, $K14^{Cre}$ X $Tbx1^{flox/flox}$($Tbx1^{K14cKO}$) embryos to study tooth and craniofacial morphogenesis. Hematoxylin and eosin (H&E) staining of sagittal sections of the craniofacial region at E16.5 demonstrated a delay in upper incisor (UI) and LI morphogenesis in $Tbx1^{K14cKO}$ mutant mice compared with WT counterparts (data not shown). The $Tbx1^{K14cKO}$ embryos at E18.5 had small LIs (~25% decrease in size, black bar compared with WT) and small LaCL regions (Fig. 6A and B). Higher magnification of the differentiating dental

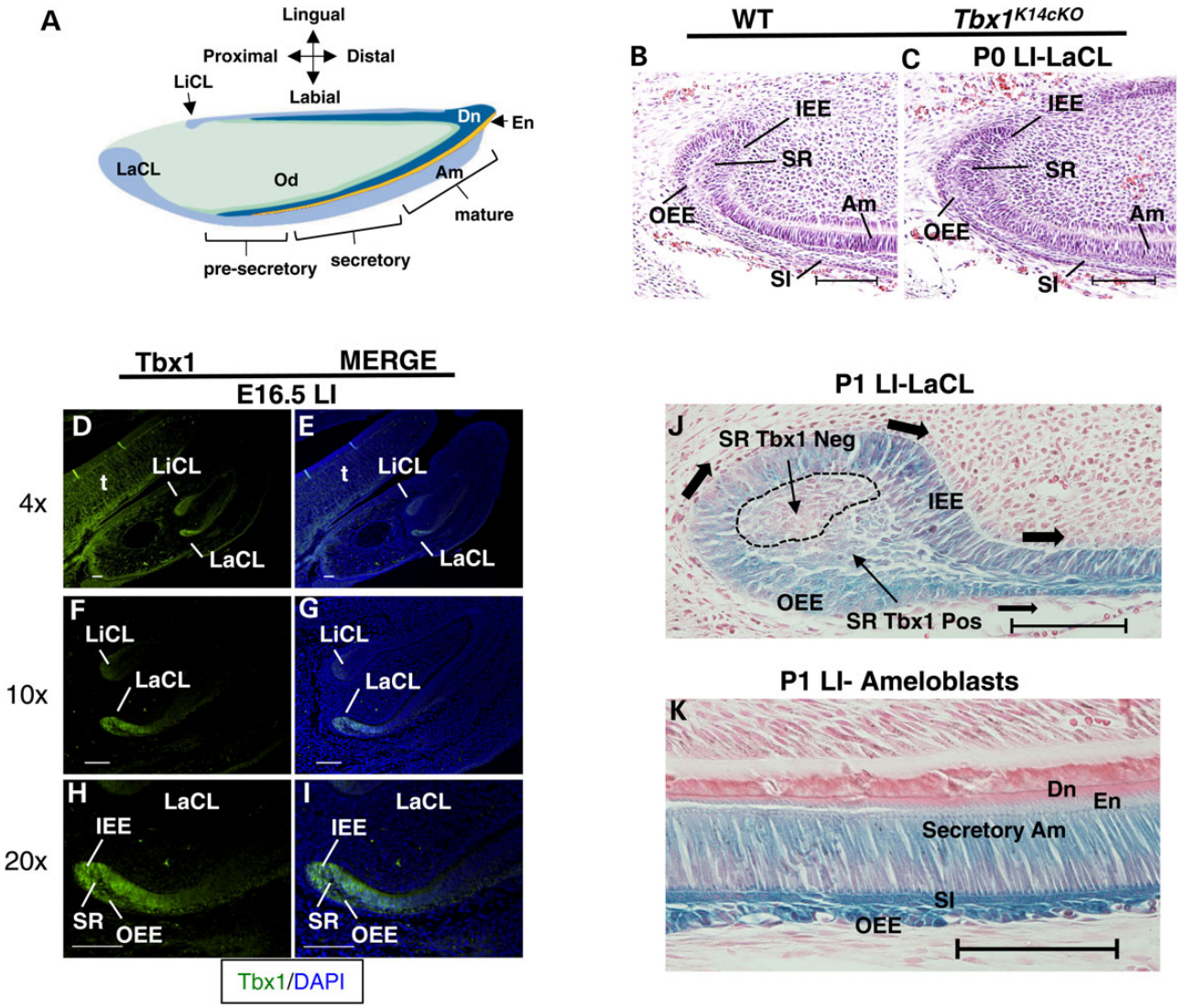

Figure 5. Tbx1 expressing cells are in a unique region of the LaCL. (**A**) Schematic representation of depiction of the mouse LI. The LaCL contains dental stem cells that supply the continuously growing mouse incisor with replacement cells. The pre-secretory, secretory and mature ameloblasts are the components that produce enamel on the labial side of the incisor. The LiCL provides cells to the growing incisor but these cells do not form ameloblasts or make enamel. Od, odontoblasts. (**B** and **C**) H&E staining of the LIs of P0 WT, and *Tbx1*^{K14cKO} mice to determine the role of Tbx1 in the LaCL. Mutant mice have smaller CLs and at P0, the cells of both the IEE and OEE are disorganized compared with their counterparts in WT mice. The SR contains the stem or progenitor cells. The SI is also thinner in the mutant mice. (**D–I**) IHC experiments show that Tbx1 is highly expressed in the LaCL and LiCL regions of the E16.5 WT LI, 2-(4-Amidinophenyl)-6-indolecarbamidine dihydrochloride, 4′,6-Diamidino-2-phenylindole dihydrochloride (DAPI) staining provides contrast. (**J**) The *Tbx1*^{Cre} *X Rosa26LacZ* mouse was analyzed for LacZ staining and Tbx1 fate mapping experiments. LacZ-positive cells are derived from Tbx1 expressing cells. In panel J, the SR compartment of the LaCL has populations of Tbx1-negative cells and Tbx1-positive cells. The Tbx1-positive cells are incorporated into the OEE and IEE, as shown by LacZ staining (the arrows denote the direction of migration of the progenitor cells). (**K**) The secretory ameloblasts and SI contain cells that expressed Tbx1 and migrated to the distal end of the incisor. These experiments were repeated three times for each embryonic stage and genotype ($N = 3$). Abbreviations: t, tongue. Scale bar = 100 μm.

epithelium (ameloblasts, Am) and dental mesenchyme (odontoblasts, Od) revealed only minor defects in both Od and Am polarization and differentiation of the LI at E18.5 in the *Tbx1*^{K14cKO} embryos (Fig. 6C and D). However, the small tooth size could have resulted from a lack of stem cell proliferation in the LaCL.

Ameloblasts are responsible for the secretion of the three structural enamel matrix proteins, amelogenin, ameloblastin and enamelin. Amelogenin constitutes ~90% of the enamel organic matrix and is highly conserved across species (38–40). Amelogenin and ameloblastin are essential for proper enamel formation (41–44). At P1, amelogenin was decreased in *Tbx1*^{K14cKO} LIs compared with WT (Fig. 6E–H). At P4, amelogenin levels in the incisors remained low or absent in the mutant mice (data not shown). The low expression of amelogenin can cause enamel defects.

H&E staining of the lower molars (LMs) at E16.5 revealed a delay in early bell stage morphogenesis in *Tbx1*^{K14cKO} embryos (data not shown). The Ek, the region where epithelial–mesenchymal signaling regulates tooth size and shape, was normal in WT mice, but underdeveloped or absent in *Tbx1*^{K14cKO} mice (data not shown). The Ek is an organizer of cusp formation and sagittal sections of P0 lower molars demonstrated defective molar cusping of the first molar (M1) in the *Tbx1*^{K14cKO} mice compared with WT mice (Fig. 6I and J). Higher magnification showed defective odontoblast (Od) and ameloblast (Am) differentiation in the *Tbx1*^{K14cKO} lower molars (Fig. 6K and L). At P4, amelogenin levels

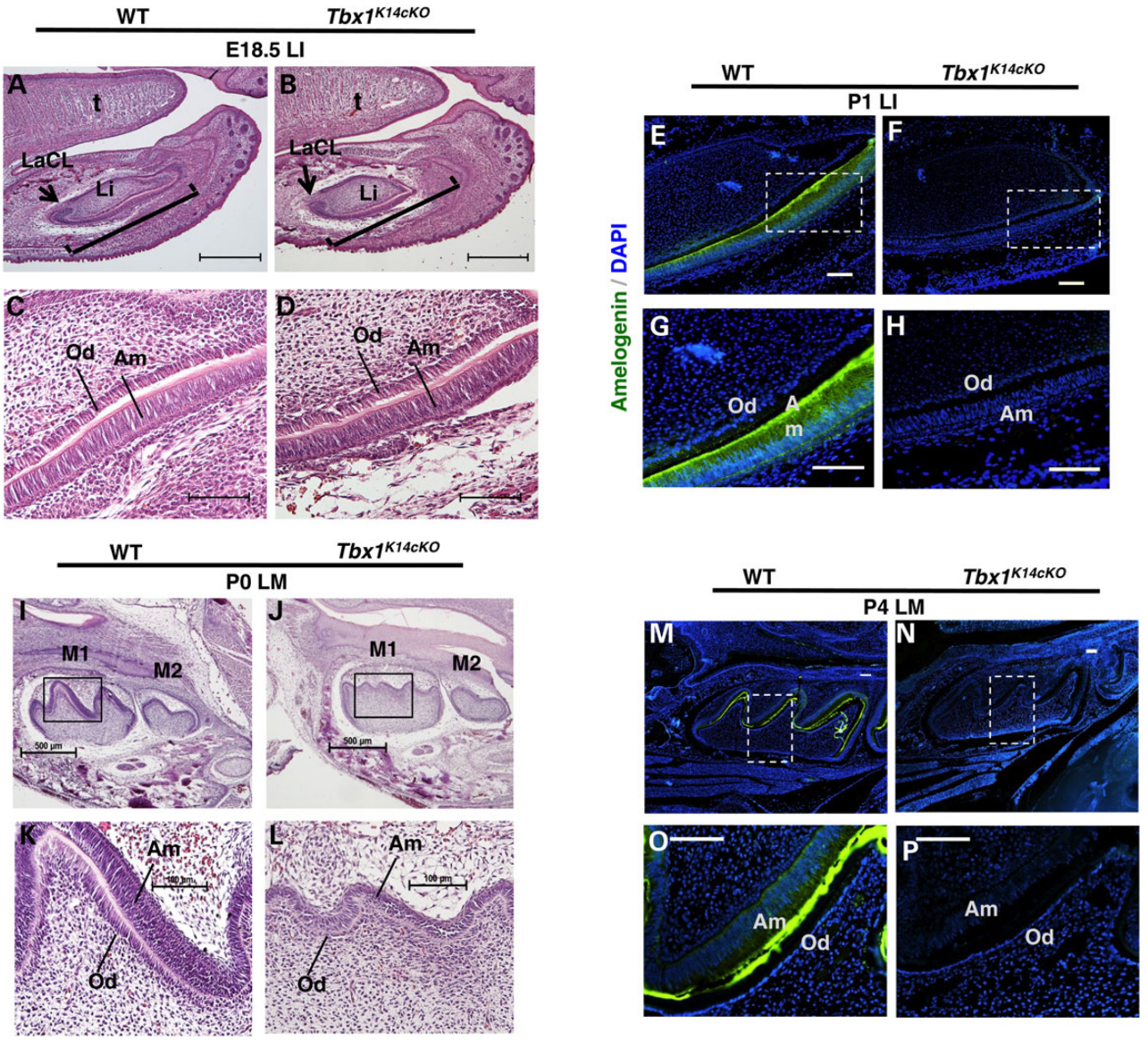

Figure 6. *Tbx1*^{K14cKO} embryos have small incisors, abnormal molar cusping with defective ameloblast differentiation and amelogenin expression. H&E staining was carried out on WT and *Tbx1*^{K14cKO} embryos at E16.5 (data not shown), E18.5 and P0. (**A** and **B**) At E18.5 the LI is small in the *Tbx1*^{K14cKO} embryos (~25% reduced compared with WT, black bar) and the portion that becomes the CL is underdeveloped (arrow). Scale bar = 100 μm. (**C** and **D**) At E18.5 the differences in Am and Od morphology compared with WT embryos is not as significant. (**E–H**) *Tbx1* mutant P1 LIs showed a decrease in amelogenin expression compared with WT (G, H, higher magnification of panels E and F, respectively). However, amelogenin is expressed in P4 *Tbx1* mutant LIs albeit at low levels (data not shown), suggesting a delay in amelogenin expression the *Tbx1*^{K14cKO} mice. (**I–L**) H&E of sagittal sections of WT and *Tbx1*^{K14cKO} mice at P0 show that the lower molar in the *Tbx1* mutant undergoes abnormal cusping. The *Tbx1*^{K14cKO} first molar (M1) has abnormal folding of the dental epithelium that gives rise to the molar cusps. Furthermore, the ameloblasts of the differentiating epithelium appears underdeveloped and undifferentiated (K and L, high magnification of panels I and J). (**M–P**) *Tbx1*^{K14cKO} mutant lower molars show decreased amelogenin expression at P4 compared with WT (O and P, higher magnification of panels M and N, respectively). These experiments were repeated three times for each genotype ($N = 3$). These experiments were repeated more than three times for each embryonic stage and genotype ($N > 3$). Abbreviations: De, dental epithelium; Am, ameloblasts; Od, odontoblasts; M1, first molar; M2, second molar. Scale bars: 100 μm.

in the molars remained low or absent in the mutant mice (Fig. 6M–P). Interestingly, ameloblastin was not diminished in *Tbx1*^{K14cKO} P4 molars and incisors (data not shown). Thus, *Tbx1*^{K14cKO} neonate mice have severely reduced amelogenin expression, but not completely absent expression.

Tbx1 regulates epithelial cell proliferation

Ki67 immunohistochemistry (IHC) was carried out on P0 WT and *Tbx1*^{K14cKO} embryos to determine if decreased cell proliferation occurred at this later stage of development. The ratio of Ki67-positive cells to the total cell number [2-(4-Amidinophenyl)-6-indolecarbamidine dihydrochloride, 4′,6-Diamidino-2-phenylindole dihydrochloride (DAPI) stain] in the LaCL was calculated to estimate the proliferation ratio. In the LI, the value for the WT LaCL was 75% and that for the mutant was 53% (Fig. 7A). These data demonstrate that the proliferation of dental stem cells in the LaCL is significantly lower in P0 mutant compared with WT neonate mice.

Mouse embryo fibroblasts (MEFs) collected from WT and *Tbx1*$^{-/-}$ mice at E14.5 were plated at 100,000 cells per 60-mm

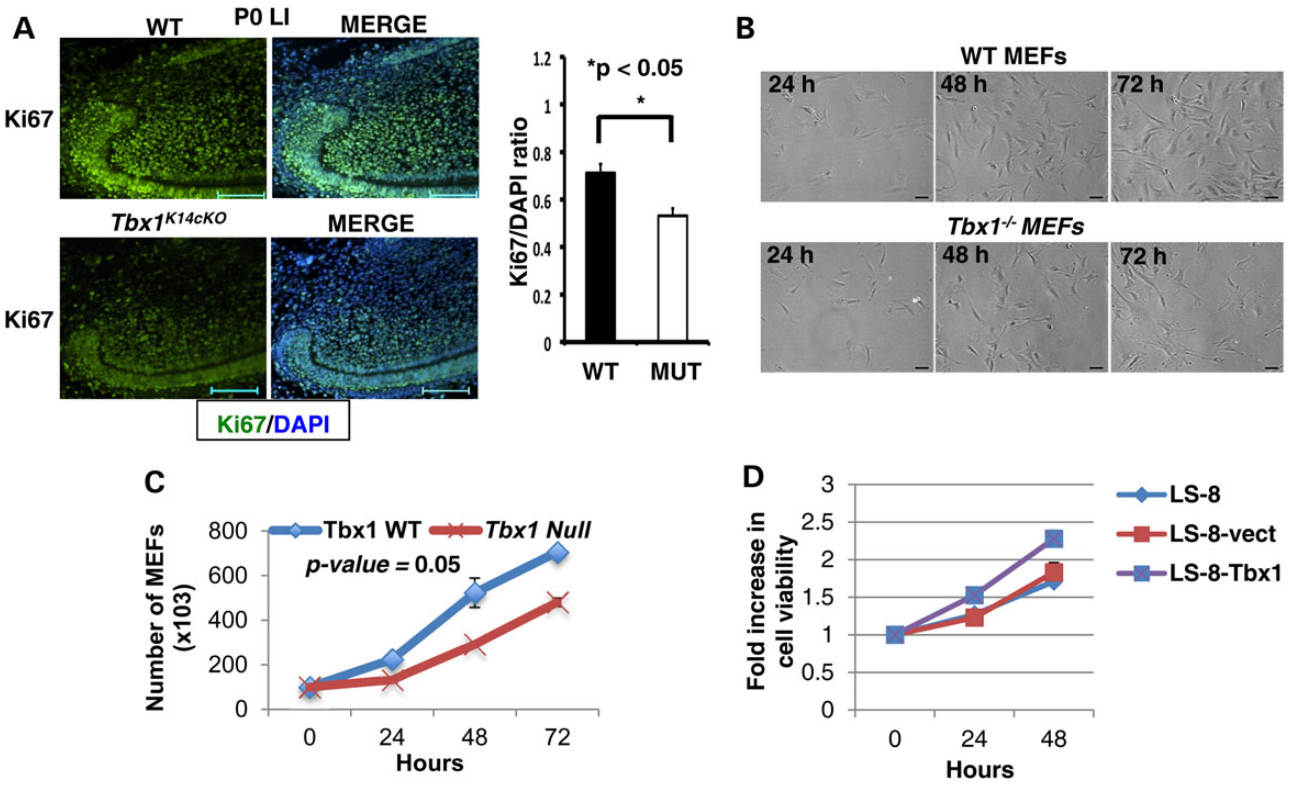

Figure 7. Tbx1 regulates cell proliferation. (**A**) LIs from WT or *Tbx1*^{K14cKO}P0 mice were processed, sectioned and stained for Ki67 to examine cell proliferation. Ki67 was decreased in *Tbx1*^{K14cKO}tooth sections, and Ki67/DAPI ratio was quantified to determine that the decrease in cell proliferation was statistically significant ($P < 0.05$). (**B**) MEFs were collected from WT and *Tbx1*$^{-/-}$ embryos at E14.5. Growth was analyzed by seeding each well with 100 000 cells, and cells were counted after 24, 48 and 72 h. MEFs extracted from *Tbx1*$^{-/-}$ embryos showed decreased cell proliferation compared with WT. (**C**) MEF cell growth was quantitated revealing a decrease in proliferation of the *Tbx1* mutant cells. Two different embryos were used for WT and *Tbx1*$^{-/-}$ and each cell count was done in triplicate. These experiments were repeated three times for each genotype. (**D**) LS-8 oral epithelial cells were transduced with a lentivirus expressing Tbx1 or empty vector. Cells were cultured for 48 h and cell growth/viability was measured every 12 h.

culture dish and counted after 24, 48 and 72 h. At each time point, *Tbx1*$^{-/-}$ MEFs proliferated more slowly than WT MEFs (Fig. 7B and C). There were no morphological changes in the MEFs between WT and *Tbx1*$^{-/-}$ mice. LS-8 oral epithelial cells were transduced with Tbx1 or vector only and cell viability/cell growth was recorded as fold increase compared with non-transduced cells. Tbx1 expressing cells demonstrated an increase in cell viability compared with WT and vector only transduced cells (Fig. 7D). Taken together, these data suggest that *Tbx1* regulates cell proliferation, and that *Tbx1* in the epithelium alone regulates tooth size by controlling cell proliferation and differentiation.

Tooth size, shape and enamel formation are reduced in adult *Tbx1*^{K14cKO} mice

Skeletal preparations of P14 WT and *Tbx1*^{K14cKO} mice were made, and scanning electron microscopy (SEM) and microCT (μCT) scans were carried out on the samples. The LIs were shorter in the mutant compared with the WT mice and the enamel layer thinner (Fig. 8A–D). At a higher magnification, the incisal edge appeared worn down or chipped in the mutant, indicating a potential decrease in enamel mineralization and/or structural defects. SEM imaging of incisors that were fractured perpendicular to the growth axis in the erupted portion of the tooth showed that the enamel layer was thinner in the mutant than the WT mice (Fig. 8E and F). At higher magnification, it became evident that the orientation of the enamel crystallite bundles (prisms) is normal in the mutant mice. However, the prisms are less densely packed and separate easily from the underlying dentin at the enamel dentine junction (Fig. 8G and H).

At P14, the first molar (M1) was smaller in the mutant (Fig. 8I–L). Also, the second molar (M2) lacked a distal cusp (Fig. 8N, O, Q, R, arrow). The cusps of the first two molars in the mutant mice were not as sharp or deep compared with WT mice (Fig. 8Q and R) and development of the third molar (M3) was more advanced in the mutant compared with WT mice (Fig. 8M–T). Overall, molars of the *Tbx1*^{K14cKO}mice were smaller (Fig. 8J and K) and featured decreased enamel formation (Fig. 8I, L, M and P), malformed cusping of the first two molars and premature growth of the third molar. The increased growth of the third molar was surprising, but may correlate to the lack of Pitx2 repression, which initiates dental development.

Tbx1 over-expression regulates incisor size and dental epithelial stem cell proliferation

Analyses of E16.5 LIs of the *K14*^{Cre} activated *Tbx1* over-expression mouse (*COET*^{K14Cre}) demonstrated a larger LaCL with less differentiated cells (Am) compared with WT mice (Fig. 9A–D). The LI of the *COET*^{K14Cre} mice is larger than that of WT at P1, with an increase in the width and length of the LaCL (Fig. 9E–H). Cell proliferation was measured by Ki67 staining of the P1 LI LaCL and

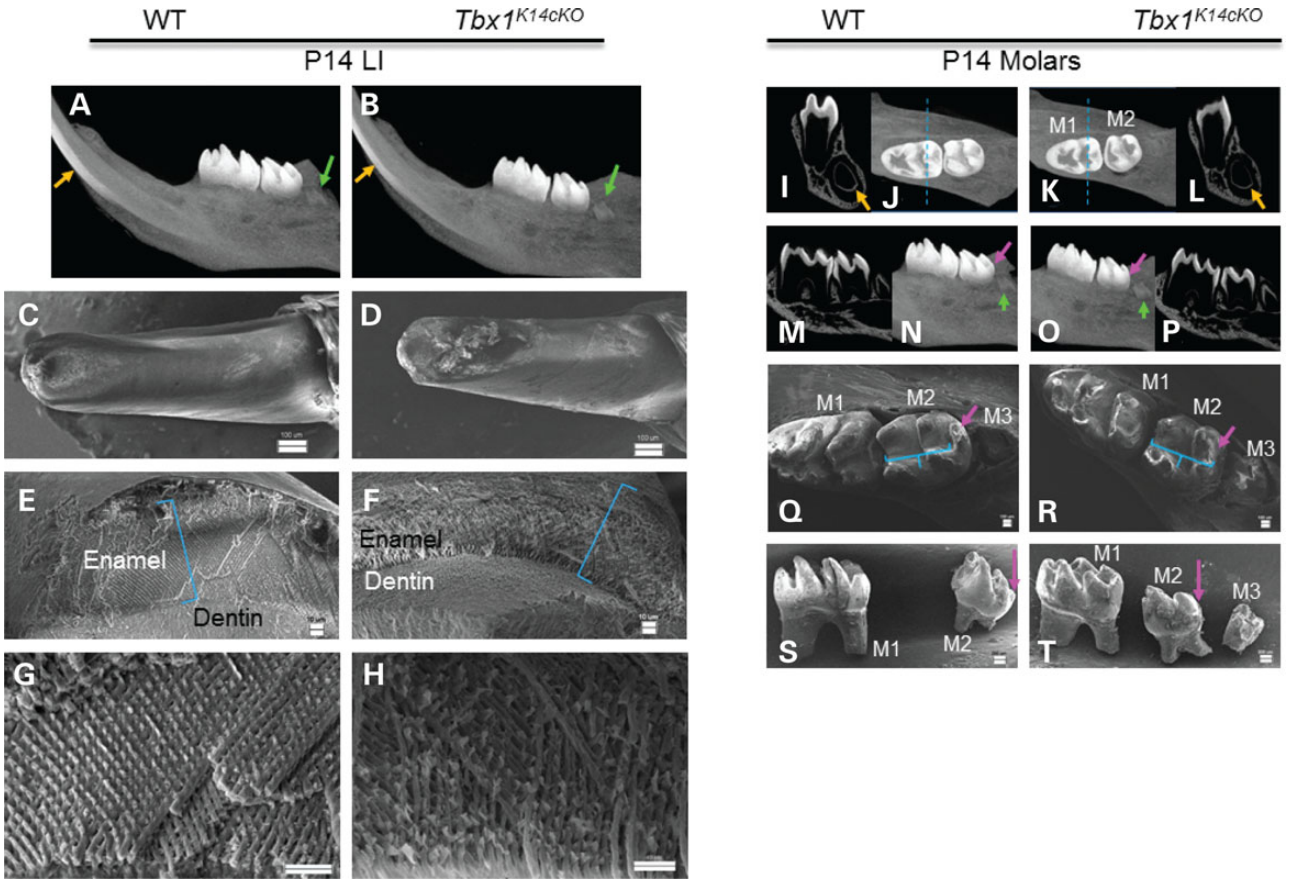

Figure 8. *Tbx1*^{K14cKO} two-week-old mice have dental anomalies and developmentally advanced third molar eruption. Skeletal preparations were performed on WT and *Tbx1*^{K14cKO} mice at P14. (**A** and **B**) μCT images of mandibles in parasagittal plane show the thinner enamel layer on the LIs (orange arrows), as well as advanced mineralization of the third molar crown in the *Tbx1*^{K14cKO} mouse compared with WT (green arrows). (**C** and **D**) SEM of the lingual side of LIs reveal smaller incisors with more wear indicating a difference in biomechanical properties of enamel, compared with WT. Scale bar 100 μm. (**E** and **F**) SEM of fracture surfaces of the erupted portion of the LI show that *Tbx1*^{K14cKO} enamel is significantly thinner as indicated by blue brackets of identical length. Scale bar 10 μm. (**G** and **H**) Mature enamel fractured at similar positions on the erupted incisor at higher magnification. Bundles of enamel crystallites (prisms) are packed densely in WT enamel but loosely with spaces between them in the *Tbx1*^{K14cKO} mouse. Scale bar 10 μm. (**I–P**) μCT scans at P14 show that mutant mice have a smaller first (M1) and second (M2) molars and a third (M3) molar that is unusually advanced in its development (green arrows). (I and L) Sections in coronal plane through the center of the distal root of the first molar, as indicated by the dotted blue line in image J and K, show differences in molar size an enamel development (less enamel mineralization on the incisor marked by orange arrow) (J and K) Maximum density projection through the mandible in transverse plane shows differences in tooth size. (M and P) Slices in parasagittal plane through the center of the distal root of the first molar and (N and O) maximum density projection in the sagittal plane show that in the mutant mice molar cusping is defective (purple arrow) and the third molar is advanced in development (green arrow). (**Q** and **R**) SEM images of whole mandibles show clearly that M2 lacks a distal cusp (purple arrow) and is smaller in the mutant mouse and that M3 has erupted and shows advanced development. Furthermore, the enamel of M1 and M2 shows signs of wear. Scale bar 100 μm. (**S** and **T**) SEM images of whole molars dissected out of the mandibles show differences in M2 cusp formation (purple arrows), similarities in root development and advanced M3 development in the mutant mouse. Scale bar 200 μm. Abbreviations: M1, first molar; M2, second molar; M3, third molar.

analyses of several mice (N = 3) revealed an increase in cell proliferation in the *COET*^{K14Cre} mice (Fig. 9I–L). These data are consistent with loss of *Tbx1* function resulting in small incisors and decreased cell proliferation in the CL regions or stem cell niche. Thus, the expression and dose of Tbx1 control dental stem cell proliferation and differentiation.

Incisor growth, amelogenin expression and enamel formation are increased with *Tbx1* over-expression

We asked if *Tbx1* over-expression increased amelogenin expression and if it correlates with an increase in enamel formation in the *COET*^{K14Cre} mice. At P1, both UIs and LIs showed increased amelogenin expression in the proximal regions compared with WT mice (Fig. 10A–H). These results suggest that Tbx1 transcriptional mechanisms may regulate amelogenin or that Tbx1 expression expands cell proliferation and increased cell differentiation.

To understand tooth structure and mineralization, we analyzed the incisors and molars of 2-week-old *COET*^{K14Cre} mice by μCT. *Tbx1* over-expression resulted in a larger incisor with increased enamel formation compared with WT (Fig. 10I and J; see arrows), and increased enamel formation (red) in the molars (Fig. 10K and L; see arrows). In *COET*^{K14Cre} mice at 4 weeks of age, the mandibles showed a decrease in alveolar bone development (Fig. 10M and N; light green arrow and orange bracket). Enamel thickness of the LI was increased in the *COET*^{K14Cre} mouse (Fig. 10M–P; blue arrow). Development of the third molar (Fig. 10O and P; yellow arrow) was delayed and cortical bone formation was decreased (Fig. 10O and P; white arrow). These results are consistent with a role for Tbx1 in regulating tooth size, shape and dental epithelial cell differentiation, which

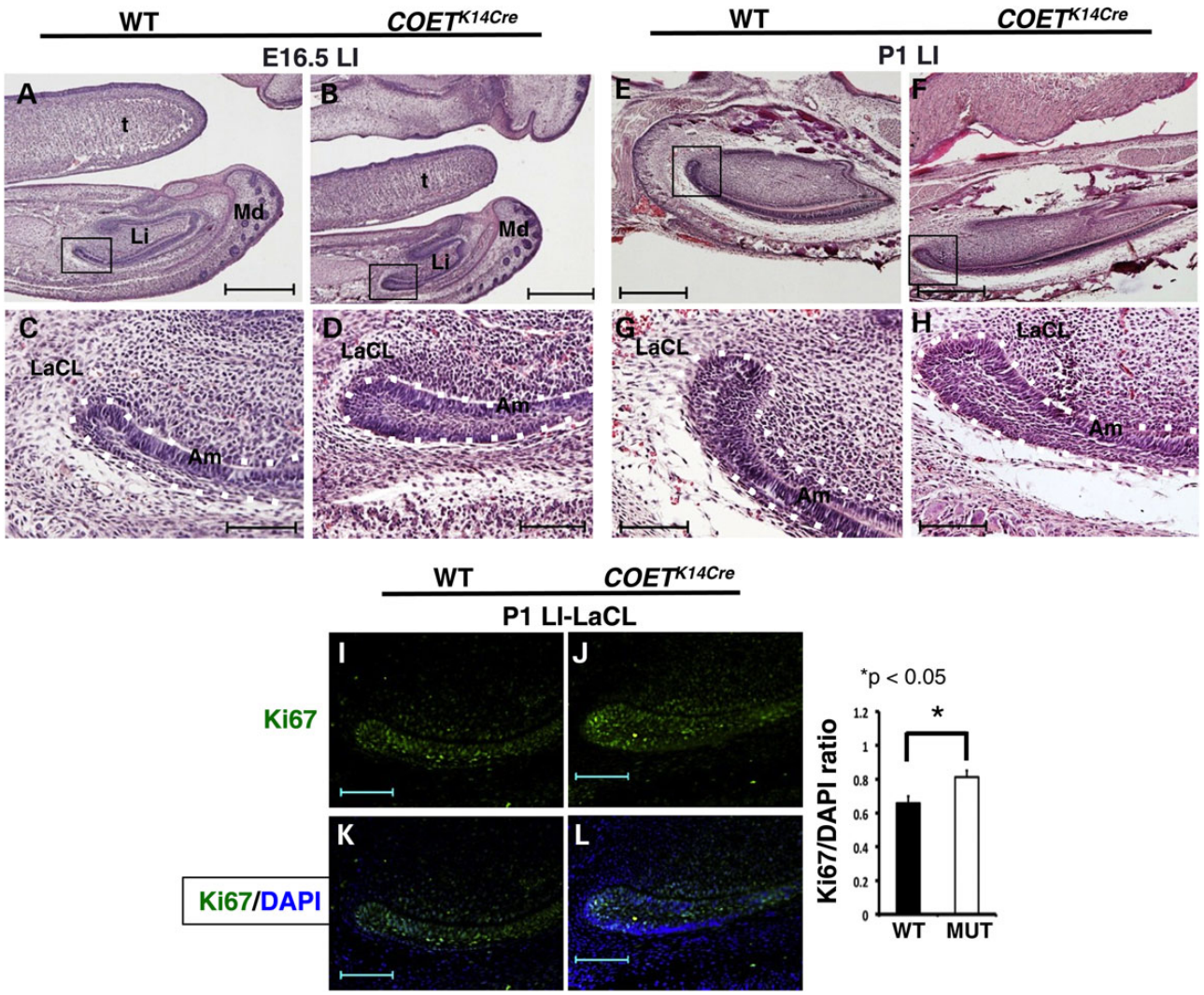

Figure 9. *Tbx1* over-expression increases incisor size and dental stem cell proliferation. (**A–D**) H&E staining of WT and $COET^{K14Cre}$ E16.5 LIs. The overall size of the incisor is similar in mice of the two genotypes at this early stage (A and B). Scale bar = 500 μm. However, the LaCL (boxed region) is larger (width and length) with an increase in cell number in the SR region of the CL and decreased ameloblast differentiation (outlined with white dotted line, higher magnification C and D). Scale bar = 100 μm. (**E–H**) H&E staining of WT and $COET^{K14Cre}$ P1 LIs. At this later stage, the $COET^{K14Cre}$ LI is larger (width and length) than its WT counterpart and the LaCL remains increased in size and shape (the LaCL is elongated in the $COET^{K14Cre}$ incisor). Scale bar = 500μm. There are more cells in the SR region of the CL in the $COET^{K14Cre}$ incisor (outlined with white dotted line, higher magnification G and H). Scale bar = 100 μm. (**I–L**) P1 LIs from WT or $COET^{K14Cre}$ mice were processed, sectioned and stained for Ki67 to assess cell proliferation. Ki67 expression was higher in the $COET^{K14Cre}$ LaCLs compared with WT, as established by quantifying the Ki67/DAPI ratio; 10 l of pups and 20 mutants were sectioned, all showed the same phenotype. Abbreviations: Am, ameloblast; t, tongue; LI, lower incisor; LaCL, labial cervical loop.

leads to enamel formation. Interestingly, third molar development was decreased in the Tbx1 over-expression mouse, which correlates to Tbx1 interaction with PITX2 to repress its transcriptional gene network required for normal dental development.

Tbx1 loss of function and gain of function embryos have cleft palate

The E16.5 $Tbx1^{K14cKO}$ embryos exhibited a cleft palate. In our *Tbx1* conditional deletion mice the palatal shelves have elevated but do not fuse (Fig. 11A and B). Interestingly, *Tbx1* over-expression also caused cleft palate in $COET^{K14Cre}$ mice (Fig. 11C and D). This is consistent with a previous report showing cleft palate in embryos over expressing *Tbx1* ($COET^{Ap2Cre}$) in the surface ectoderm (45). The palatal shelves appeared to elevate but did not fuse at the midline.

Discussion

The cloning and characterization of *Tbx1* in mice established this gene as essential for embryonic development. To understand the role of *Tbx1* in odontogenesis, gene and miR expression was analyzed in WT, $Tbx1^{K14cKO}$ and $COET^{K14Cre}$ embryonic stage-specific mouse mandibles, maxilla and dental epithelial tissue. Bioinformatics analyses of the expression data revealed genes and miRs regulated by *Tbx1*. Comparison of increased gene expression with decreased miR expression or the inverse in these tissues revealed tentative correlations of miR-regulated gene expression controlled by *Tbx1*. A regulatory loop was identified between *Tbx1* and *miR-96*, which further correlated with their expression patterns in the developing incisor epithelium. To further establish a potential link to 22q11.2DS, several *TBX1* mutants were assayed for their transcriptional activity and their ability to regulate the genes and miRs identified in the bioinformatics screens. The

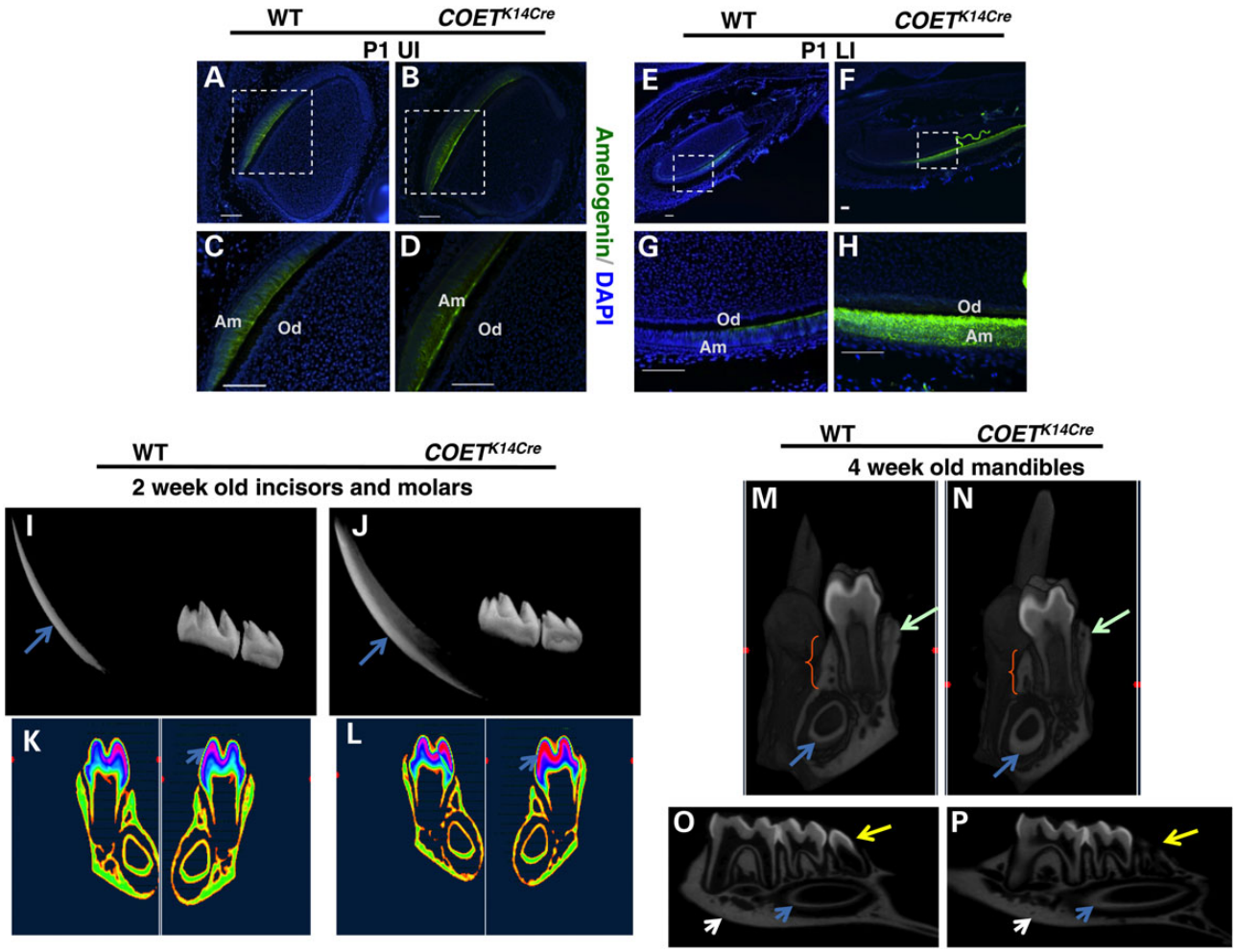

Figure 10. *Tbx1* over-expression increases amelogenin, enamel formation and a delay in formation of the third molar. (**A–D**) WT and $COET^{K14Cre}$ P1 UIs were sectioned and stained for the expression of amelogenin. Amelogenin expression was increased in the $COET^{K14Cre}$ UI (higher magnification, compare C, WT to D, $COET^{K14Cre}$ sections). (**E–H**) Amelogenin expression was increased in the $COET^{K14Cre}$LI (higher magnification, compare G, WT to H, $COET^{K14Cre}$ sections). (**I–L**) μCT imaging shows an increase in the size and shape of the P14 (2 weeks old) $COET^{K14Cre}$ incisor compared with its WT counterpart (I and J). The enamel on the labial side is thicker in the $COET^{K14Cre}$ incisor (blue arrow). Imaging of the P14 mandible (left and right sides) shows an increase in molar enamel formation (blue arrow) and a slight loss of alveolar and cortical bone formation in the $COET^{K14Cre}$ mandible (green color, K, L). (**M** and **N**) microCT analyses of P28 mandibles show an increase in enamel formation (blue arrow) in the incisor of the $COET^{K14Cre}$ mice, coincident with a decrease in alveolar bone formation (light green arrow and orange brackets). (**O** and **P**) microCT scans of the hemimandible show a developmental delay in formation of the third molar (yellow arrow), a decreased in formation of cortical bone (white arrow) and an increase in formation of incisor enamel in the $COET^{K14Cre}$ incisor (blue arrow).

TBX1 mutations were analyzed in cell-based assays to understand their function compared with WT *TBX1*. The *in vivo* bioinformatics approach identified direct targets of *Tbx1* in mouse models for 22q11.2DS and these targets could account for the molecular underpinnings of dental and craniofacial anomalies observed in DiGeorge patients. Clearly some Tbx1 molecular mechanisms between humans and mouse models are different however using the approach in this report revealed new genetic pathways potentially associated with 22q11.2DS.

TBX1, 22q11.2DS and associated dental anomalies

TBX1 is a candidate gene for 22q11.2DS and is responsible for the majority of the phenotypes seen in 22q11.2DS patients. Various clinical studies have shown that 22q11.2DS patients have tooth defects, ranging from hypodontia to enamel defects (3). Independent of the role of TBX1 in the pharyngeal apparatus, epithelial *Tbx1* expression in a maturing tooth has been shown to be specific to the IEE, and cells in this region become mature ameloblasts that secrete enamel (10).

Dental anomalies such as enamel hypoplasia and hypomineralization, hypodontia and aberrant tooth shape are documented in 22q11.2DS patients (3). Tooth defects in 22q11.2DS patients have been linked to hypocalcemia from hypoplasia of the parathyroid, and by micrognathia. Traditionally, enamel disturbances in 22q11.2DS patients were thought to be secondary effects of hypocalcemia caused by hypoparathyroidism. A recent study concluded that a diagnosis of hypoparathyroidism did not affect the prevalence of enamel anomalies (46). Thus, our research demonstrates that the dental and craniofacial defects in 22q11.2DS patients involve a gene regulatory network modulated by Tbx1 regulating cell proliferation and differentiation.

Tbx1–protein interactions regulate development

Pitx2, a bicoid/paired-related homeobox gene, was initially identified as the mutated gene in the autosomal-dominant, haploinsufficient Axenfeld-Rieger syndrome (47). Patients with this disorder display many tooth abnormalities, including dental

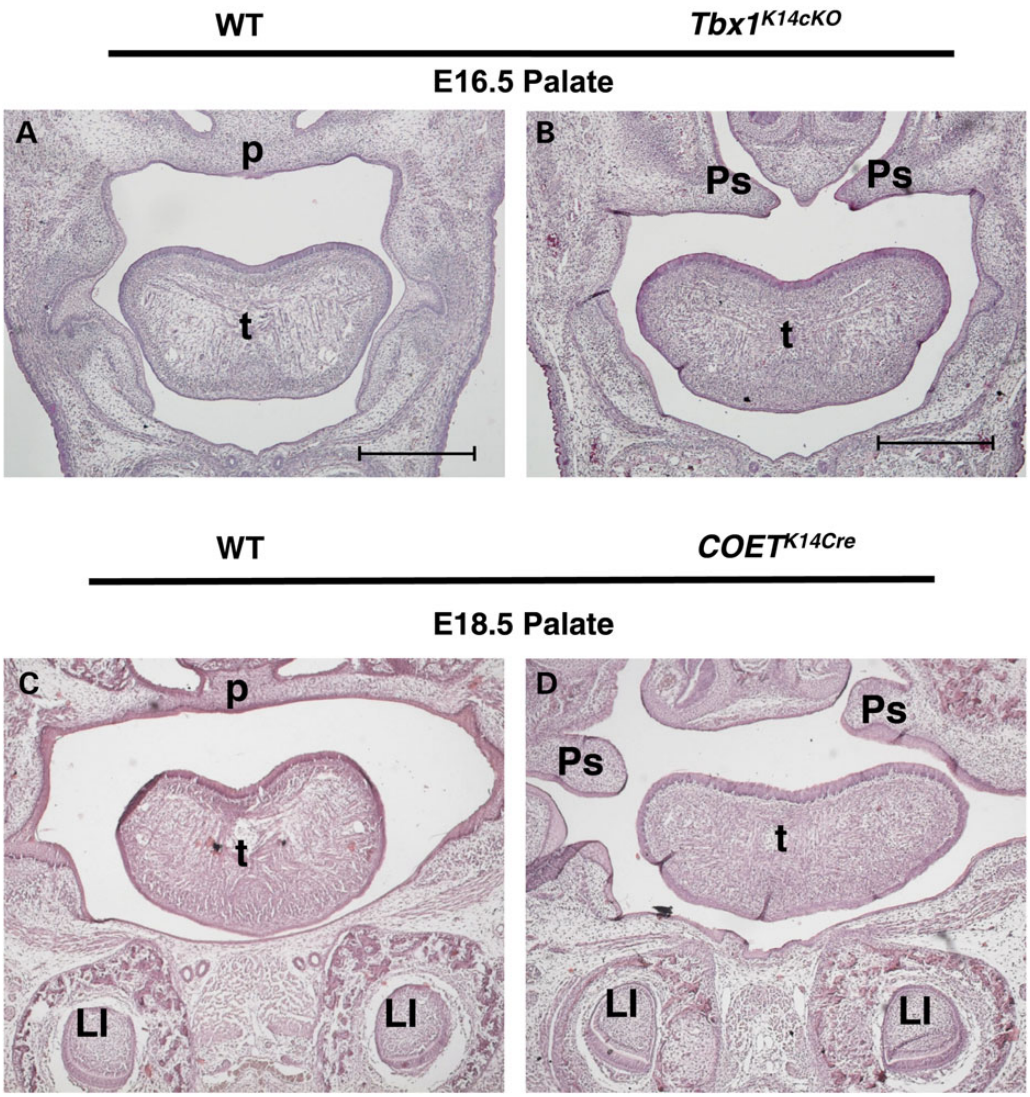

Figure 11. *Tbx1* loss-of-function and gain-of-function mice have cleft palate. (**A** and **B**) At E16.5 $Tbx1^{K14cKO}$ mice have a cleft palate shown by coronal sections of the anterior palate. (**C** and **D**) Coronal sections of $COET^{K14Cre}$ mice at E18.5 show that *Tbx1* over-expression causes cleft palate. These experiments were repeated more than three times for each embryonic stage and genotype ($N > 3$). Abbreviations: LI, lower incisor; t, tongue; Ps, palatal shelves; p, palate. Scale bar = 500 μm.

hypoplasia, abnormally shaped teeth and anodontia vera. Within the craniofacial region, *Pitx2* is the earliest detected transcription factor in the oral epithelium, and the expression patterns of *Tbx1* and *Pitx2* overlap during tooth morphogenesis (48,49). *Tbx1* represses *PITX2*-mediated activation of the cyclin-dependent kinase inhibitor p21 in teeth by physically interacting with the PITX2 C-terminus, providing a molecular mechanism for the proliferation of dental epithelial cells (24).

A recent study identified a hierarchical network of transcription factors expressed in the pharyngeal mesoderm that coordinates both heart and craniofacial development. This network includes genetic interactions between *Tbx1*, *Pitx2*, *Lhx2*, *Tcf21* and *bHLH* genes (14,50). This study suggests that Tbx1 levels can be fine-tuned by interactions with other transcription factors, and that these factors may be modifiers for 22q11.2DS (50).

We have dissected the role of Tbx1 protein domains and their interaction with PITX2 to demonstrate that the Tbx1 N-terminus is required for PITX2 binding and repression of PITX2 transcriptional activity. Tbx1 repression of PITX2 during tooth development may regulate tooth initiation and the size and shape of both incisors and molars. We have shown previously that $Pitx2^{-/+}/Tbx1^{-/+}$ double het mice form an extra premolar, demonstrating that these two factors interact genetically to regulate tooth initiation and formation (24). In this report, we show that $Tbx1^{K14cKO}$ mice have increased third molar development while the $COET^{K14Cre}$ mice have decreased third molar development, suggesting that the dose of Tbx1 regulates tooth initiation and the timing of tooth development. Because TBX1 is a potent regulator of PITX2 transcriptional activity, which initiates tooth development, the TBX1–PITX2 interaction appears to control tooth initiation and patterning. Tbx1 is expressed early during tooth development and is co-expressed with Pitx2 in the developing incisor and molar. Tbx1 and Pitx2 are early regulators of a gene expression network that define cell proliferation and differentiation of several cell types.

Human TBX1 and DGS associated mutations also regulate PITX2 transcriptional activity. Both TBX1 H194Q and TBX1 G310S proteins are stable and not degraded in cells. TBX1 G310S represses PITX2 activation but at reduced levels compared with WT TBX1; however, TBX1 H194Q has no effect on PITX2 activity.

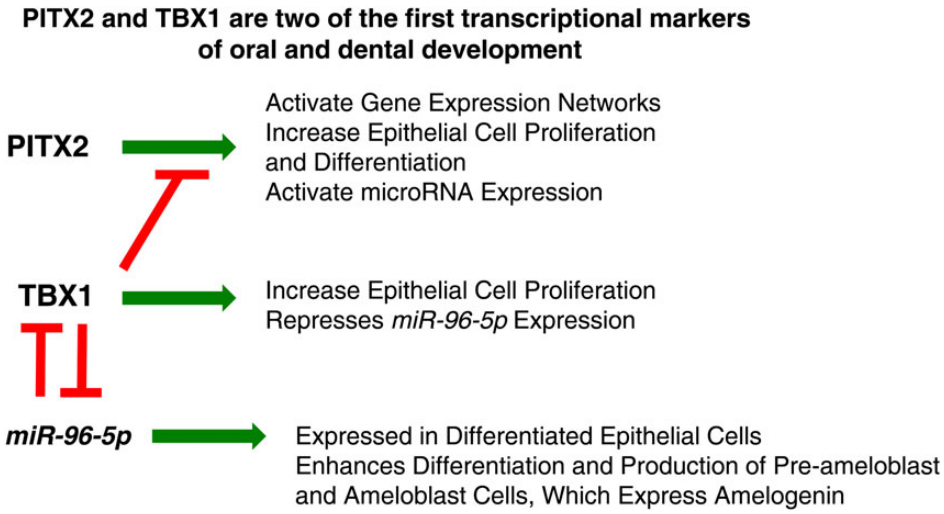

Figure 12. Model for the role of Tbx1 in tooth and craniofacial development. PITX2 and TBX1 are two of the first transcription markers for dental development and both a co-expressed in the early dental epithelium, dental lamina and oral epithelium. PITX2 is a transcriptional activator, which activates a gene regulatory network required for dental development (62). TBX1 can repress PITX2 transcriptional activity, but also activate other genes required for cell proliferation. TBX1 is part of a negative feedback loop with miR-96. TBX1 represses miR-96 expression and miR-96 represses TBX1 expression. This feedback loop allows dental epithelial cells to differentiate and produce ameloblasts, which express amelogenin.

The TBX1 N-terminal tail is highly conserved in all three isoforms while the C-terminal tail varies (51). Because the interaction between PITX2 and TBX1 is crucial for embryonic craniofacial development, it makes sense that PITX2 binds to a highly conserved portion of TBX1. Both TBX1 H194Q and G310S mutations were predicted to affect TBX1 DNA binding and protein stabilization (25), however neither is affected in the mutant proteins, (27) and our study. However, both mutations may alter dimer formation and/or protein function (25). However, these mutations do not appear to change the N-terminal structure of the TBX1 protein, which binds PITX2. Thus other mechanisms are likely responsible for their differential transcriptional activity.

Tbx1 in palatogenesis

Craniofacial malformations occur in more than half of 22q11.2DS patients, and cleft palate (complete, submucosal and soft) is one of the most frequent features (52). *Tbx1*-null mice exhibited abnormal epithelial adhesion between the palate and the mandible, leading to clefts similar to those observed in 22q11.2DS (53,54). However, during palate development it was suggested that *Tbx1*-null epithelium was hyperproliferative and did not differentiate and that Tbx1 over-expression inhibited cell growth (53). Funato *et al.* suggested that *Tbx1* regulated the balance between proliferation and differentiation in the epithelium of the palatal primordial (53). Our studies demonstrate that both loss and gain of *Tbx1* function causes clefting supporting the dose-dependent regulation of palatogenesis and development by *Tbx1*. However, during odontogenesis Tbx1 acts to increase epithelial cell proliferation consistent with a role for Tbx1 in regulating dental epithelial progenitor cells. This is also consistent with the role of Tbx1 in cardiac progenitor cells where it increases proliferation and inhibits differentiation (55).

Tbx1 in odontogenesis

The CL regions (stem niche) of both UIs and LIs displayed decreased proliferation in $Tbx1^{K14cKO}$ mice and increased proliferation in the $Tbx1^{K14COET}$ mice. These data demonstrated that *Tbx1* is essential for maintenance of dental progenitor cells. When *Tbx1* ($Tbx1^{K14cKO}$) was conditionally deleted from the oral and dental epithelia, we observed microdontia, underdeveloped CLs and defective ameloblast differentiation and these effects can be explained by a decrease in the proliferation of progenitor cells.

The size of the developed incisors and molars appeared smaller in the $Tbx1^{K14cKO}$ mice at P14 and P20. In molars a distal cusp is missing in the second molar. These abnormalities may be explained by decreased progenitor cells in the LaCL and delayed formation of the Ek. Both incisors and molars show wear of the enamel layer, and on close examination, the enamel prisms formed are less dense than in WT mice, especially in the region closest to the enamel–dentin junction (EDJ). Tbx1 regulates the timing of ameloblast differentiation and the subsequent production of enamel proteins, and the effect seen is a delay and not a complete absence of enamel production.

Tbx1 expression has been shown to be restricted to the IEE at E12.5 and is maintained by mesenchyme-derived Fgf signaling (56). Tbx1 and Fgf8 interact genetically during development (57). However, using $Tbx1^{Cre}$ fate mapping we demonstrate that Tbx1 expressing cells are located in a unique and distinct region of the LaCL during incisor development. It appears that Tbx1 expressing cells are located in a defined region of the SR that may define both lineages of the pre-ameloblast cells and cells of the OEE and SI. Sox2 expressing cells mark a region of the LaCL that appear not to express Tbx1 (36). We define this region as Tbx1 negative, which suggests that Tbx1 marks a cell lineage separate from Sox2. However, more experiments are required to determine the exact differences.

Tbx1 and *microRNA* regulation

miRs have been shown to be essential regulators of embryogenesis. Bmp signaling promotes outflow tract (OFT) myocardial differentiation by regulating miRs (58). Bmp signals through a conserved Smad-binding element to regulate *miR-17-92*, which results in decreased *Tbx1* expression. Smad1 is a critical negative regulator of SHF proliferation *in vivo*, and ablation of Smad1 in the SHF enhances cell proliferation (59). Tbx1 binds to Smad1 and

negatively modulates the Bmp-Smad signaling pathway by interfering with the Smad1–Smad4 interaction (45). A bidirectional negative feedback loop connecting Bmp, Smad, *miR-17-92* and Tbx1 may regulate heart development. A recent paper showed that Tbx1 acts as an on–off switch for Bmp signaling in the hair follicles, acting as a regulator of stem cells transitioning between the quiescent and proliferative states (60). Furthermore, a nice study recently demonstrated that *miR-17-92* null mice have craniofacial defects including cleft palate and that Tbx1 was a target of *miR-17-92* (61). Tbx1 also inhibits Bmp signaling in the incisor LaCL to prevent immature ameloblast differentiation (unpublished data).

We hypothesized that miRs play a role in ameloblast proliferation and differentiation by regulating the expression of *Tbx1*. *miR-96* is expressed in the mouse incisor LaCL, but at low levels. This might reflect regulation of its expression by factors in the LaCL (20). We demonstrate that Tbx1 repressed *miR-96* expression, which maintains the expression of *miR-96* at low levels in the LaCL. Such control is important for Tbx1 regulation of the dental stem cell niche (Fig. 12). However, increased *miR-96* expression may be required to repress Tbx1 to produce differentiated ameloblasts, but we cannot rule out that other factors may either activate *miR-96* or repress *Tbx1* expression in ameloblasts. *miR-96* indirectly regulates Pitx2 expression and transcriptional activity by inhibiting Tbx1 expression and the ability of Tbx1 to repress Pitx2 transcriptional activation. This would modulate Pitx2 transcriptional activity and fine-tune dental and craniofacial development and the gene regulatory network activated by Pitx2. miRs act as modulators of gene networks to define the timing of gene expression and the patterns of expression. We demonstrate that *miR-96* defines the expression pattern of Tbx1 in the LaCL, where Tbx1 expression is high and *miR-96* is low. However, in the ameloblasts where *miR-96* expression increased it facilitates decreased Tbx1 expression and cell differentiation. This is a great example of the dose response of miRs and transcription factors in regulating cell proliferation versus differentiation during development.

TBX1 G310S mutant protein represses the *miR-96* promoter, however, TBX1 H194Q does not repress or activate the *miR-96* promoter. The change in *miR-96* expression could modulate craniofacial and dental development. Human mutations in the *miR-96* seed region, disrupting its function, are associated with progressive hearing loss through the modulation of gene expression in hair cells affecting their normal function (63). Therefore, the altered TBX1-*miR-96* regulatory loop is a candidate to explain the dental defects such as enamel hypoplasia, hypomineralization, hypodontia and aberrant tooth shape documented in 22q11.2DS patients.

Tbx1 regulates dental stem cell proliferation and differentiation controlled by *miR-96*. Our data suggest that Tbx1 regulates a unique set of progenitor cells during dental development. We have uncovered potential molecular underpinnings for the tooth defects in patients with 22q11.2DS. The human *TBX1* mutations result in altered proteins that cannot effectively repress PITX2 activity and modulate *miR-96* expression.

Materials and Methods

Animals

All animals were housed at the University of Iowa, in the Program of Animal Resources and were handled in accordance with the principles and procedure of the Guide for the Care and Use of Laboratory Animals. All experimental procedures were approved by the University of Iowa IACUC guidelines. $Tbx1^{+/-}$ (64), $Tbx1^{flox/+}$ (65), $Tbx1^{Cre}$ (15,66), COET (Conditional Over-expression of Tbx1) (12), $K14^{Cre}$ (18) and $ROSA26^{LacZ}$ (Jackson Labs) were previously described. Observation of a vaginal plug was counted as embryonic (E) day 0.5, and embryos were collected at E14.5, E16.5, E18.5, P0 and P4. Mice and embryos from WT, $K14^{Cre}$; $Tbx1^{flox/flox}$($Tbx1^{K14cKO}$) were genotyped from DNA extraction of tail biopsies. Mice and embryos were genotyped by PCR using DNA extracted from tail biopsies and previously published PCR primers.

Cell proliferation and MTT assays

Mouse embryonic fibroblasts (MEFs) were obtained from E14.5 WT and mutant mice. MEFs were passaged twice and plated at 100 000 cells per 60-mm cultured plate. Cell numbers were counted at 24, 48 and 72 h time points.

Tbx1, empty vector or non-transduced LS-8 cells were plated in triplicate at 5000, 2500, 1250 and 625 cells/well in 96 well plates. After 4 h, when 98% of the cells had adhered, the media was removed from one plate (0 h) and 100 µl of media + MTT (Thiazolyl blue tetrazolium bromide, Sigma) were added to 0.12 mM and allowed to incubate at 37°C for 4 h. After 4 h, 100 µl of 1% SDS and 0.1 N HCl were added to the wells and the plate was further incubated at 37°C for 4 h. Plates were then analyzed on a microtiter plate reader at 570 nm. Plates were compared for 0, 24 and 48 h. Values at 0 h were set to 1 and the fold increase was calculated at 24 and 48 h. Each point cell dilution was done in triplicate and the experiment was done twice ($n = 2$).

Histology and IHC

Embryonic heads were fixed in 4% paraformaldehyde (PFA) for 0.5–4 h at room temperature (RT). Samples were dehydrated with increasing concentrations of ethanol, followed by xylene, embedded in paraffin and sectioned at 7-µm thickness. H&E staining was used to examine craniofacial and tooth morphology. For IHC, sections were de-paraffinized and boiled with 0.1 M sodium citrate buffer for 15 min and cooled in solution to RT. Slides were blocked with 10% serum for 1 h followed by overnight incubation at 4°C with anti-amelogenin (Santa Cruz, 1:200), anti-ameloblastin (Santa Cruz, 1:200), anti-Tbx1 (Invitrogen, 1:200) and anti-Ki67 (Abcam, 1:200). For fluorescein immunochemistry (IF), secondary antibodies conjugated to FITC were used at a dilution of 1:200 (Invitrogen). DAPI was used for counter staining. For IHC, slides were treated with a biotinylated goat anti-rabbit IgG conjugate (Vector Labs, 1:200) using the avidin–biotin complex (Vector Labs) and an AEC staining kit (Sigma).

Fluorescence immunocytochemistry

For cell-based IF, cells were seeded on cover slides for 24 h, followed by fixation with cold acetone for 5 min. Cells were washed twice with PBS-Tween (PBS-T) and incubated with 10% goat serum for 30 min at RT and then incubated with 1/500 Myc-tagged Ab (Cell Signaling) or 1/250 Beta-catenin Ab (Santa Cruz) for 2 h at RT. Cells were washed three times in PBS-T and then incubated with Alexa-488 or Alexa-555 at 1/250 for 30 min at RT. Finally, the cells were washed three times with PBS-T for 10 min each, and counter stained using mounting solution containing DAPI.

Cell culture, transient transfection, luciferase and β-galactosidase assays

Tbx1 expression plasmid was previously described (65,67). *miR-96* expression plasmid was constructed as previously described for

other miRs (68). The *pre-miR-96* was cloned into the expression vector. The *Tbx1 3′UTR* was cloned after the luciferase gene in pGL3 vector (Promega) (68). Truncations of the mouse *Tbx1* gene were made using sequence-specific primers to Tbx1 by PCR with *Eco*RI and *Kpn*I restriction enzyme sites. Tbx1 FL (full length), Tbx1 ΔC (deletion of C-Terminal tail) and Tbx1 ΔN (deletion of N-terminus) were cloned into pcDNA3.1. The *Pitx2c* luciferase promoter construct has been previously described (24), and the 5 kb *miR-96* promoter was PCR amplified from mouse genomic DNA and cloned into the luciferase plasmid. All plasmid constructs were confirmed by DNA sequencing. LS-8 (oral epithelial) cells (69) were cultured in 10% fetal bovine serum (FBS) and 1% penicillin/streptomycin and transfected via electroporation as previously described (70). Cells were fed fresh media 24 h before transfection, and electroporated with 2.5 μg of expression plasmid, 5 μg of reporter plasmid and 0.5 μg of SV-40 β-galactosidase plasmid. Transfected cells were incubated for 48 h in 60-mm culture dishes, lysed and assayed for β-galactosidase activity (Tropix Inc.), luciferase activity (Promega) and protein content (Bio-Rad). All luciferase activities were normalized to β-galactosidase activity and protein concentration. Experiments were repeated three to five times and the results are shown ±SEM. Transfection protocol for *miR-96* to knock down endogenous Tbx1 used 1 μg DNA, 3 μl of X-tremeGene HP DNA transfection reagent, 200 μl of serum free media and LS-8 cells in a 6-well plate. Cells were plated at 10–20% confluence and harvested after 48 h and assayed for endogenous Tbx1 expression by western blot.

Expression and purification of GST-Tbx1 mutants and GST-PITX2A fusion proteins

Cloning of *Tbx1* and *PITX2A* into pGEX6P-2 GST vector was previously described (24,71). *Tbx1* deletion constructs were PCR amplified from a cDNA clone and ligated into pGEX6P-2 GST vector (Amersham Pharmacia Biotech, Piscataway, NJ) using *Eco*RI and *Xho*I restriction enzyme sites. The plasmids were confirmed by DNA sequencing and transformed in BL21 cells. Proteins were extracted as previously described (71,72). PITX2A was cleaved from GST moiety using 80 units of PreScission protease (Pharmacia Biotech) per milliliter of glutathione sepharose. Protein concentrations were quantified with Bradford Reagent (Bio-Rad Laboratories, Hercules, CA) and stored in 10% glycerol. Commassie Blue staining of denatured SDS-polyacrylamide gels was used to verify production of protein.

GST pull-down assays

Immobilized GST-Tbx1, GST-Tbx1ΔNT, GST-Tbx1ΔTC, GST-Tbx1ΔC and GST-Tbx1Tbox fusion proteins were suspended in binding buffer (20 mM HEPES, pH 7.5, 5% glycerol, 50 mM NaCl, 1 mM Ethylenediaminetetraacetic acid, 1 mM Dithiothreitol, 1% milk and 400 μg/ml of ethidium bromide). Purified bacteria expressed PITX2A (500 ng) was added to 15 μg immobilized GST-Tbx1 FL and truncated constructs, incubated for 30 min at 4°C. The beads were washed 5× with 200 μl binding buffer. The bound proteins were eluted by boiling for 5 min in SDS-sample buffer and separated on a 10% SDS-polyacrylamide gel. The proteins were then transferred to polyvinylidene difluoride (PVDF) filters, immunoblotted and detected using PITX2ABCDE antibody (Capra Science, Sweden) and ECL reagents.

Western blotting

Expression of transiently expressed Tbx1 was demonstrated using a 1:500 dilution of anti-myc antibody (Cell Signaling). Approximately 15–40 μg of cell lysates were used for sodium dodecyl sulfate gel electrophoresis. The protein was transferred to PVDF filters (Millipore), immunoblotted and detected using specific secondary antibodies and enhanced-chemiluminescene ECL reagents (GE HealthCare).

Quantitative real-time PCR of *mRNA* and *microRNA*

Total RNA and miR from MEFs, LS-8, CHO and HEK 293 FT cells were prepared using the miRNeasy Mini Kit (Qiagen). The quantity and integrity of the RNA samples were assessed by measurements at 260 and 280 nm and verified using gel analysis. LIs and molars from E18.5 control and $Tbx1^{K14COET}$ were also dissected and all of the RNA was prepared using the miRNeasy Mini Kit (Qiagen). MicroRNA were reversed transcribed using TaqMan microRNA assay probes (Applied Biosystems) and the TaqMan microRNA reverse transcription kit (Applied Biosystems) according to the manufacturer's instruction. Quantitative real-time PCR (qPCR) analysis of miRs was performed using TaqMan microRNA assay probes and normalized using the U6B probe (Taqman Universal PCR mastermix, Applied Biosystems).

Total RNA was reversed transcribed into cDNA using oligo (dT) primers according to the manufacturer's instructions (iScript Select cDNA Synthesis Kit, Bio-Rad). The MyiQ single colored Real-Time Detection System (Bio-Rad) was used for the reactions, and quantities were analyzed using the MyiQ Optical System Software 2.0 (Bio-Rad). cDNA levels were normalized to *β-actin* (F: 5′-GCCTTCCTTCTTGGGTATG-3′ and R: 5′-ACCACCAGACAGC ACTGTG-3′). Primers used for qPCR are as follows: *Tbx1* (F: 5′-CGA CAAGCTGAAACTGACCA-3′ and R: 5′-GTGACTGCAGTGAAGC GTGT-3′) and *Sox2* (F: 5′-ATGAGAGCAAGTACTGGCAAG-3′ and R: 5′-TCGGCAGCCTGATTCCAATAA-3′). The thermal cycling profile consisted of 95°C for 4 min, 40 cycles of denaturation at 95°C for 30 s, annealing at 60°C for 30 s and elongation at 72°C for 30 s. Samples were run in triplicate. Melting curves were generated to confirm the amplification specificity of the PCR products. In addition, all of the PCR products were sequenced to verify that the correct band was amplified.

Statistical analysis

For each condition, three experiments were performed and the results are presented as the mean ± SEM. The differences between two groups of conditions were analyzed using an independent, two-tailed *t*-test.

SEM imaging and microCT

Hemi-mandibles of littermate WT and $Tbx1^{K14cKO}$, *COET* or $Tbx1^{Pitx2cKO}$ were dissected, fixed in 4% PFA overnight in 4°C and stored in 70% ethanol. EM images of uncoated specimens were taken with a Zeiss Evo LS 10 scanning electron microscope (Carl Zeiss, Peabody, USA) in secondary electron mode at 7 kV, 3 pA under high vacuum to assess gross morphology. Subsequently the incisors and molars were fractured, mounted on stubs using adhesive copper tape, and gold coated (Denton V Sputter coater, Denton, Moorestown, NJ). Images were then collected in secondary electron mode at 10 kV and 8 pA in high vacuum mode and at a working distance of 5–9 mm. MicroCT samples were analyzed in ethanol using a MicroCT 40 (Scanco Medical, Brüttisellen, Switzerland) at 70 kV, 114 μA, 8 W and 10 μm resolution, with an integration time of 300 ms. All samples to be compared were scanned in one batch to ensure identical conditions and allow for comparison of mineral densities. The images in DICOM format were processed

using Fiji imaging software (http://fiji.sc/Fiji) to standardize the orientation of the samples. All samples were processed identically, setting an arbitrary, but identical threshold to remove any background and to allow for a comparison of mineral densities between samples in slices and maximum intensity projections.

ChIP assay

ChIP assays were performed as previously described (73,74) using the Zymo-Spin ChIP kit (Zymo research) using LS8 cells. Specific PCR amplification of the putative Tbx1 site in the *miR-96* promoter was performed using the following primers (-133 and -384 away from the *miR-96* predicted start): 5′-TGAAAGGTGGG CTCGG-3′ and 5′-CCTTCTAGGTTTCCTGCT-3′. As a control, PCR analysis was performed on ChIP samples using primers upstream of the putative Tbx1 site using the following primers (+384 and +512 from the *miR-96* predicted start site): 5′-GGCC AAGGAAGTCAGGAAT-3′ and 5′-TAGTTCCTCGGGTGTGGACT-3′.

Acknowledgements

We thank members of Amendt and Baldini Laboratories for helpful discussions and Christine Blaumueller for editorial expertise. We thank the Forsyth Institute for microCT imaging and analyses and Dr James Martin, Baylor College of Medicine, for reagents.

Conflict of Interest statement. None declared.

Funding

Support for this research was provided by funds from the University of Iowa and grant DE 13941 from the National Institute of Dental and Craniofacial Research to B.A.A.

References

1. Goldberg, R., Motzkin, B., Marion, R., Scambler, P.J. and Shprintzen, R.J. (1993) Velo-cardio-facial syndrome: a review of 120 patients. *Am. J. Med. Genet.*, **45**, 313–319.
2. Shprintzen, R.J., Goldberg, R.B., Lewin, M.L., Sidoti, E.J., Berkman, M.D., Argamaso, R.V. and Young, D. (1978) A new syndrome involving cleft palate, cardiac anomalies, typical facies, and learning disabilities: velo-cardio-facial syndrome. *Cleft Palate J.*, **15**, 56–62.
3. Klingberg, G., Oskarsdottir, S., Johannesson, E.L. and Noren, J.G. (2002) Oral manifestations in 22q11 deletion syndrome. *Int. J. Paediatr. Dent.*, **12**, 14–23.
4. Lindsay, E.A. (2001) Chromosomal microdeletions: dissecting del22q11 syndrome. *Nat. Rev. Genet.*, **2**, 858–868.
5. Jerome, L.A. and Papaioannou, V.E. (2001) DiGeorge syndrome phenotype in mice mutant for the T-box gene, Tbx1. *Nat. Genet.*, **27**, 286–291.
6. Merscher, S., Funke, B., Epstein, J.A., Heyer, J., Puech, A., Lu, M. M., Xavier, R.J., Demay, M.B., Russell, R.G., Factor, S. *et al.* (2001) TBX1 is responsible for cardiovascular defects in velo-cardio-facial/DiGeorge syndrome. *Cell*, **104**, 619–629.
7. Bollag, R.J., Siegfried, Z., Cebra-Thomas, J.A., Garvey, N., Davison, E.M. and Silver, L.M. (1994) An ancient family of embryonically expressed mouse genes sharing a conserved protein motif with the T locus. *Nat. Genet.*, **7**, 383–389.
8. Arnold, J.S., Werling, U., Braunstein, E.M., Liao, J., Nowotschin, S., Edelmann, W., Hebert, J.M. and Morrow, B.E. (2006) Inactivation of Tbx1 in the pharyngeal endoderm results in 22q11DS malformations. *Development*, **133**, 977–987.
9. Nowotschin, S., Liao, J., Gage, P.J., Epstein, J.A., Campione, M. and Morrow, B.E. (2006) Tbx1 affects asymmetric cardiac morphogenesis by regulating Pitx2 in the secondary heart field. *Development*, **133**, 1565–1573.
10. Zoupa, M., Seppala, M., Mitsiadis, T. and Cobourne, M.T. (2006) Tbx1 is expressed at multiple sites of epithelial–mesenchymal interaction during early development of the facial complex. *Int. J. Dev. Biol.*, **50**, 504–510.
11. Zhang, Z. and Baldini, A. (2008) In vivo response to high-resolution variation of Tbx1 mRNA dosage. *Hum. Mol. Genet.*, **17**, 150–157.
12. Vitelli, F., Huynh, T. and Baldini, A. (2009) Gain of function of Tbx1 affects pharyngeal and heart development in the mouse. *Genesis*, **47**, 188–195.
13. Liao, J., Kochilas, L., Nowotschin, S., Arnold, J.S., Aggarwal, V. S., Epstein, J.A., Brown, M.C., Adams, J. and Morrow, B.E. (2004) Full spectrum of malformations in velo-cardio-facial syndrome/DiGeorge syndrome mouse models by altering Tbx1 dosage. *Hum. Mol. Genet.*, **13**, 1577–1585.
14. Kong, P., Racedo, S.E., Macchiarulo, S., Hu, Z., Carpenter, C., Guo, T., Wang, T., Zheng, D. and Morrow, B.E. (2014) Tbx1 is required autonomously for cell survival and fate in the pharyngeal core mesoderm to form the muscles of mastication. *Hum. Mol. Genet.*, **23**, 4215–4231.
15. Huynh, T., Chen, L., Terrell, P. and Baldini, A. (2007) A fate map of Tbx1 expressing cells reveals heterogeneity in the second cardiac field. *Genesis*, **45**, 470–475.
16. Harada, H., Kettunen, P., Jung, H.S., Mustonen, T., Wang, Y.A. and Thesleff, I. (1999) Localization of putative stem cells in dental epithelium and their association with Notch and FGF signaling. *J. Cell Biol.*, **147**, 105–120.
17. Harada, H., Toyono, T., Toyoshima, K., Yamasaki, M., Itoh, N., Kato, S., Sekine, K. and Ohuchi, H. (2002) FGF10 maintains stem cell compartment in developing mouse incisors. *Development*, **129**, 1533–1541.
18. Cao, H., Wang, J., Li, X., Florez, S., Huang, Z., Venugopalan, S.R., Elangovan, S., Skobe, Z., Margolis, H.C., Martin, J.F. *et al.* (2010) MicroRNAs play a critical role in tooth development. *J. Dent. Res.*, **89**, 779–784.
19. Jevnaker, A.M. and Osmundsen, H. (2008) MicroRNA expression profiling of the developing murine molar tooth germ and the developing murine submandibular salivary gland. *Arch. Oral Biol.*, **53**, 629–645.
20. Jheon, A.H., Li, C.-Y., Wen, T., Michon, F. and Klein, O.D. (2011) Expression of micrornas in the stem cell niche of the adult mouse incisor. *PLoS ONE*, **6**, e24536.
21. Michon, F., Tummers, M., Kyyronen, M., Frilander, M.J. and Thesleff, I. (2010) Tooth morphogenesis and ameloblast differentiation are regulated by micro-RNAs. *Dev. Biol.*, **340**, 355–368.
22. Cao, H., Jheon, A., Li, X., Sun, Z., Wang, J., Florez, S., Zhang, Z., McManus, M.T., Klein, O.D. and Amendt, B.A. (2013) The Pitx2: miR-200c/141:noggin pathway regulates Bmp signaling and ameloblast differentiation. *Development*, **140**, 3348–3359.
23. Gay, I., Cavender, A., Peto, D., Sun, Z., Speer, A., Cao, H. and Amendt, B.A. (2013) Differentiation of human dental stem cells reveals a role for microRNA-218. *J. Periodontal Res.*, **49**, 110–120.
24. Cao, H., Florez, S., Amen, M., Huynh, T., Skobe, Z., Baldini, A. and Amendt, B.A. (2010) Tbx1 regulates progenitor cell proliferation in the dental epithelium by modulating Pitx2 activation of p21. *Dev. Biol.*, **347**, 289–300.
25. Zweier, C., Sticht, H., Aydin-Yaylagul, I., Campbell, C.E. and Rauch, A. (2007) Human TBX1 missense mutations cause

gain of function resulting in the same phenotype as 22q11.2 deletions. *Am. J. Med. Genet.*, **80**, 510–517.
26. Paylor, R., Glaser, B., Mupo, A., Atallotis, P., Spencer, C., Sobotka, A., Sparks, C., Choi, C.H., Oghalai, J. and Curran, S., *et al.* (2006) Tbx1 haploinsufficiency is linked to behavioral disorders in mice and humans: implications for 22q11 deletion syndrome. *Proc. Natl. Acad. Sci. USA*, **103**, 7729–7734.
27. Castellanos, R., Xie, Q., Zheng, D., Cvekl, A. and Morrow, B.E. (2014) Mammalian TBX1 preferentially binds and regulates downstream targets via a tandem T-site repeat. *PLoS ONE*, **9**, e95151.
28. Chieffo, C., Garvey, N., Gong, W., Roe, B., Zhang, G., Silver, L., Emanuel, B.S. and Budarf, M.L. (1997) Isolation and characterization of a gene from the DiGeorge chromosomal region homologous to the mouse Tbx1 gene. *Genomics*, **43**, 267–277.
29. Gong, W., Gottlieb, S., Collins, J., Blescia, A., Dietz, H., Goldmuntz, E., McDonald-McGinn, D.M., Zackai, E.H., Emanuel, B.S., Driscoll, D.A. *et al.* (2001) Mutation analysis of TBX1 in non-deleted patients with features of DGS/VCFS or isolated cardiovascular defects. *J. Med. Genet.*, **38**, E45.
30. Byrne, C., Tainsky, M. and Fuchs, E. (1994) Programming gene expression in developing epidermis. *Development*, **120**, 2369–2383.
31. Dassule, H.R., Lewis, P., Bei, M., Maas, R. and McMahon, A.P. (2000) Sonic hedgehog regulates growth and morphogenesis of the tooth. *Development*, **127**, 4775–4785.
32. Takamori, K., Hosokawa, R., Xu, X., Deng, X., Bringas, J. P. and Chai, Y. (2008) Epithelial fibroblast growth factor receptor 1 regulates enamel formation. *J. Dent. Res.*, **87**, 238–243.
33. Mitsiadis, T.A. and Drouin, J. (2008) Deletion of the Pitx1 genomic locus affects mandibular tooth morphogenesis and expression of the Barx1 and Tbx1 genes. *Dev. Biol.*, **313**, 887–896.
34. Caton, J., Luder, H.U., Zoupa, M., Bradman, M., Bluteau, G., Tucker, A.S., Klein, O. and Mitsiadis, T.A. (2009) Enamel-free teeth: Tbx1 deletion affects amelogenesis in rodent incisors. *Dev. Biol.*, **328**, 493–505.
35. Thesleff, I. and Tummers, M. (2009) Tooth Organogenesis and Regeneration. *The Stem Cell Research Community, StemBook*, StemBook, ed.
36. Juuri, E., Saito, K., Ahtiainen, L., Seidel, K., Tummers, M., Hochedlinger, K., Klein, O.D., Thesleff, I. and Michon, F. (2012) Sox2+ stem cells contribute to all epithelial lineages of the tooth via Sfrp5+ progenitors. *Dev. Cell*, **23**, 317–328.
37. Bei, M. (2009) Molecular genetics of ameloblast cell lineage. *J. Exp. Zool. B Mol. Dev. Evol.*, **312B**, 437–444.
38. Fincham, A.G., Moradian-Oldak, J. and Simmer, J.P. (1999) The structural biology of the developing dental enamel matrix. *J. Struct. Biol.*, **126**, 270–299.
39. Nakahori, Y., Takenaka, O. and Nakagome, Y. (1991) A human X–Y homologous region encodes 'amelogenin'. *Genomics*, **9**, 264–269.
40. Snead, M.L., Lau, E.C., Zeichner-David, M., Fincham, A.G., Woo, S.L. and Slavkin, H.C. (1985) DNA sequence for cloned cDNA for murine amelogenin reveal the amino acid sequence for enamel-specific protein. *Biochem. Biophys. Res. Commun.*, **129**, 812–818.
41. Gibson, C.W. (2011) The amelogenin proteins and enamel development in humans and mice. *J. Oral Biosci.*, **53**, 248–256.
42. Wright, J.T., Hart, T.C., Hart, P.S., Simmons, D., Suggs, C., Daley, B., Simmer, J., Hu, J., Bartlett, J.D., Li, Y. *et al.* (2009) Human and mouse enamel phenotypes resulting from mutation or altered expression of AMEL, ENAM, MMP20 and KLK4. *Cells Tissues Organs*, **189**, 224–229.
43. Gibson, C.W. (1999) Regulation of amelogenin gene expression. *Crit. Rev. Eukaryot. Gene Expr.*, **9**, 45–57.
44. Fukumoto, S., Kiba, T., Hall, B., Iehara, N., Nakamura, T., Longenecker, G., Krebsbach, P.H., Nanci, A., Kulkarni, A.B. and Yamada, Y. (2004) Ameloblastin is a cell adhesion molecule required for maintaining the differentiation state of ameloblasts. *J. Cell Biol.*, **167**, 973–983.
45. Fulcoli, F.G., Huynh, T., Scambler, P.J. and Baldini, A. (2009) Tbx1 regulates the BMP-Smad1 pathway in a transcription independent manner. *PLoS ONE*, **4**, e6049.
46. Nordgarden, H., Lima, K., Skogedal, N., Følling, I., Storhaug, K. and Abrahamsen, T.G. (2012) Dental developmental disturbances in 50 individuals with the 22q11.2 deletion syndrome; relation to medical conditions? *Acta Odontol. Scand.*, **70**, 194–201.
47. Semina, E.V., Reiter, R., Leysens, N.J., Alward, L.M., Small, K. W., Datson, N.A., Siegel-Bartelt, J., Bierke-Nelson, D., Bitoun, P., Zabel, B.U. *et al.* (1996) Cloning and characterization of a novel bicoid-related homeobox transcription factor gene, RIEG, involved in Rieger syndrome. *Nat. Genet.*, **14**, 392–399.
48. Liu, W., Selever, J., Lu, M.F. and Martin, J.F. (2003) Genetic dissection of Pitx2 in craniofacial development uncovers new functions in branchial arch morphogenesis, late aspects of tooth morphogenesis and cell migration. *Development*, **130**, 6375–6385.
49. Lin, C.R., Kioussi, C., O'Connell, S., Briata, P., Szeto, D., Liu, F., Izpisua-Belmonte, J.C. and Rosenfeld, M.G. (1999) Pitx2 regulates lung asymmetry, cardiac positioning and pituitary and tooth morphogenesis. *Nature*, **401**, 279–282.
50. Harel, I., Maezawa, Y., Avraham, R., Rinon, A., Ma, H.Y., Cross, J.W., Leviatan, N., Hegesh, J., Roy, A., Jacob-Hirsch, J. *et al.* (2012) Pharyngeal mesoderm regulatory network controls cardiac and head muscle morphogenesis. *Proc. Natl. Acad. Sci. USA*, **109**, 18839–18844.
51. Yagi, H., Furutani, Y., Hamada, H., Sasaki, T., Asakawa, S., Minoshima, S., Ichida, F., Joo, K., Kimura, M., Imamura, S. *et al.* (2003) Role of TBX1 in human del22q11.2 syndrome. *Lancet*, **362**, 1366–1373.
52. Marom, T., Roth, Y., Goldfarb, A. and Cinamon, U. (2012) Head and neck manifestations of 22q11.2 deletion syndromes. *Eur. Arch. Otorhinolaryngol.*, **269**, 381–387.
53. Funato, N., Nakamura, M., Richardson, J.A. and Srivastava, D. (2012) Tbx1 regulates oral epithelial adhesion and palatal development. *Hum. Mol. Genet.*, **21**, 2524–2537.
54. Goudy, S., Law, A., Sanchez, G., Baldwin, H.S. and Brown, C. (2010) Tbx1 is necessary for palatal elongation and elevation. *Mech. Dev.*, **127**, 292–300.
55. Chen, L., Fulcoli, F.G., Tang, S. and Baldini, A. (2009) Tbx1 regulates proliferation and differentiation of multipotent heart progenitors. *Circ. Res.*, **105**, 842–851.
56. Mitsiadis, T.A., Tucker, A.S., De Bari, C., Cobourne, M.T. and Rice, D.P.C. (2008) A regulatory relationship between Tbx1 and FGF signaling during tooth morphogenesis and ameloblast lineage determination. *Dev. Biol.*, **320**, 39–48.
57. Vitelli, F., Taddei, I., Morishima, M., Meyers, E.N., Lindsey, E.A. and Baldini, A. (2002) A genetic link between Tbx1 and fibroblast growth factor signaling. *Development*, **129**, 4605–4611.
58. Wang, J., Greene, S.B., Bonilla-Claudio, M., Tao, Y., Zhang, J., Bai, Y., Huang, Z., Black, B.L., Wang, F. and Martin, J.F. (2010) Bmp signaling regulates myocardial differentiation from cardiac progenitors through a MicroRNA-mediated mechanism. *Dev. Cell*, **19**, 903–912.

59. Prall, O.W., Menon, M.K., Solloway, M.J., Watanabe, Y., Zaffran, S., Bajolle, F., Biben, C., McBride, J.J., Robertson, B.R., Chaulet, H. *et al.* (2007) An Nkx2.5/Bmp2/Smad1 negative feedback loop controls heart progenitor specification and proliferation. *Cell*, **128**, 947–959.
60. Chen, T., Heller, E., Beronja, S., Oshimori, N., Stokes, N. and Fuchs, E. (2012) An RNA interference screen uncovers a new molecule in stem cell self-renewal and long-term regeneration. *Nature*, **485**, 104–108.
61. Wang, J., Bai, Y., Li, H., Greene, S.B., Klysik, E., Yu, W., Schwartz, R.J., Williams, T.J. and Martin, J.F. (2013) MicroRNA-17-92, a direct Ap-2α transcriptional target, modulates T-box factor activity in orofacial clefting. *PLoS Genet.*, **9**, e1003785.
62. Sharp, T., Wang, J., Li, X., Cao, H., Gao, S., Moreno, M. and Amendt, B.A. (2014) A pituitary homeobox 2 (Pitx2):microRNA-200a-3p:beta-catenin pathway converts mesenchyme cells to amelogenin-expressing dental epithelial cells. *J. Biol. Chem.*, **289**, 27327–27341.
63. Mencía, A., Modamio-Høybjør, S., Redshaw, N., Morín, M., Mayo-Merino, F., Olavarrieta, L., Aguirre, L.A., del Castillo, I., Steel, K.P., Dalmay, T. *et al.* (2009) Mutations in the seed region of human miR-96 are responsible for nonsyndromic progressive hearing loss. *Nat. Genet.*, **41**, 609–613.
64. Lindsay, E.A., Vitelli, F., Su, H., Morishima, M., Huynh, T., Pramparo, T., Jurecic, V., Ogunrinu, G., Sutherland, H.F., Scambler, P.J. *et al.* (2001) Tbx1 haploinsufficieny in the DiGeorge syndrome region causes aortic arch defects in mice. *Nature*, **410**, 97–101.
65. Xu, H., Morishima, M., Wylie, J.N., Schwartz, R.J., Bruneau, B. G., Lindsay, E.A. and Baldini, A. (2004) Tbx1 has a dual role in the morphogenesis of the cardiac outflow tract. *Development*, **131**, 3217–3227.
66. Vitelli, F., Morishima, M., Taddei, I., Lindsay, E.A. and Baldini, A. (2002) Tbx1 mutation causes multiple cardiovascular defects and disrupts neural crest nerve migratory pathways. *Hum. Mol. Genet.*, **11**, 915–922.
67. Amen, M., Liu, X., Vadlamudi, U., Elizondo, G., Diamond, E., Engelhardt, J.F. and Amendt, B.A. (2007) PITX2 and beta-catenin interactions regulate Lef-1 isoform expression. *Mol. Cell Biol.*, **27**, 7560–7573.
68. Zhang, Z., Florez, S., Gutierrez-Hartmann, A., Martin, J.F. and Amendt, B.A. (2010) MicroRNAs regulate pituitary development, and microRNA 26b specifically targets lymphoid enhancer factor 1 (Lef-1), which modulates pituitary transcription factor 1 (Pit-1) expression. *J. Biol. Chem.*, **285**, 34718–34728.
69. Chen, L.S., Couwenhoven, R.I., Hsu, D., Luo, W. and Snead, M. L. (1992) Maintenance of amelogenin gene expression by transformed epithelial cells of mouse enamel organ. *Archs. Oral Biol.*, **37**, 771–778.
70. Green, P.D., Hjalt, T.A., Kirk, D.E., Sutherland, L.B., Thomas, B. L., Sharpe, P.T., Snead, M.L., Murray, J.C., Russo, A.F. and Amendt, B.A. (2001) Antagonistic regulation of Dlx2 expression by PITX2 and Msx2: implications for tooth development. *Gene Expr.*, **9**, 265–281.
71. Amendt, B.A., Sutherland, L.B. and Russo, A.F. (1999) Multifunctional role of the Pitx2 homeodomain protein C-terminal tail. *Mol. Cell Biol.*, **19**, 7001–7010.
72. Cox, J.C., Hayhurst, A., Hesselberth, J., Bayer, T.S., Georgiou, G. and Ellington, A.D. (2002) Automated selection of aptamers against protein targets translated in vitro: from gene to aptamer. *Nuc. Acids Res.*, **30**, e108.
73. Venugopalan, S.R., Li, X., Amen, M.A., Florez, S., Gutierrez, D., Cao, H., Wang, J. and Amendt, B.A. (2011) Hierarchical interactions of homeodomain and forkhead transcription factors in regulating odontogenic gene expression. *J. Biol. Chem.*, **286**, 21372–21383.
74. Li, X., Venugopalan, S., Cao, H., Pinho, F., Paine, M.L., Snead, M.L., Semina, E.V. and Amendt, B.A. (2013) A model for the molecular underpinnings of tooth defects in Axenfeld-Rieger Syndrome. *Hum. Mol. Genet.*, **23**, 194–208.